10-2017

A Hierarchical Approach for Creating Electrically Conductive Network Structure in Polyurethane Nanocomposites using a Hybrid of Graphene Nanoplatelets, Carbon Black and Multi-Walled Carbon Nanotubes

Pashupati Pokharel
University of New Haven

Dequan Xiao
University of New Haven, DXiao@NewHaven.edu

Folarin Erogbogbo
San Jose State University

Ozgur Keles
San Jose State University

Dai Soo Lee
Chonbuk National University

Publisher Citation

Pokharel P, Xiao D, Erogbogbo F, Keles O, Lee DS, A hierarchical approach for creating electrically conductive network structure in polyurethane nanocomposites using a hybrid of graphene nanoplatelets, carbon black and multi-walled carbon nanotubes, Composites Part B (2018), doi: https://doi.org/10.1016/j.compositesb.2018.10.057.

Comments

This is the authors' accepted manuscript of the article published in *Composites Part B*. The version of record can be found at https://doi.org/10.1016/j.compositesb.2018.10.057.

Electrically conductive network structure in polyurethane nanocomposites using a hybrid of graphene nanoplatelets, carbon black and multi-walled carbon nanotubes

Pashupati Pokharel [a,*], Dequan Xiao [a], Folarin Erogbogbo [b], Ozgur Keles [b], Dai Soo Lee [c]

[a] Center for Integrative Materials Discovery, Department of Chemistry and Chemical Engineering, University of New Haven, Boston Post Road, West Haven 06516, Connecticut, USA

[b] Biomedical, Chemical and Material Engineering, San Jose State University, Washington Square, San Jose, California, USA

[c] Department of Semiconductors and Chemical Engineering, Chonbuk National University, Jeonju 561-756, Republic of Korea.

*Corresponding author, e-mail address: ppokharel2008@gmail.com ppokharel@newhaven.edu, Tel:2034794189, Fax: 2039316077

ABSTRACT

Hierarchical organization of carbon nanomaterials is the best strategy to combine desirable factors and synergistically impart mechanical and electrical properties to polymers. Here, we investigate the relaxation behavior of carbon nanofillers filled polyurethane (PU) with special reference to particle size and aspect ratio, filler morphology, filler loading to understand the conductive network formation of fillers in the PU matrix. Typically, an addition of 2 wt% hybrid fillers of graphene nanoplatelets (GNPs), conductive carbon black (CB) and multi-walled carbon nanotubes (MWCNTs) in PU at 1:1:2 mass ratio (GCM112-PU2) showed lowest surface resistivity ~$10^{6.8}$ ohm/sq along with highest improved mechanical properties. Our results demonstrate how hierarchical compositions may function in polymer configurations that are useful for thermal and electrical systems.

Keywords: Nano-structures; Nanocomposites; Electrical properties; Stress relaxation

1. Introduction

In the nanocomposites research, a lot of emphasis has been placed on the study of carbon nanofillers, including but not limited to, carbon nanotubes (CNTs) and graphene[1–5]. The high electrical conductivity, high aspect ratio and cylindrical shape of CNTs, have made them interesting components for the preparation of conductive polymer nanocomposites [6,7]. The use of CNTs in nanocomposites has been limited by the challenges in maintaining their properties after processing, dispersing them in polymers, and producing them cost effectively [8]. Solving problems that result in the cost-effective fabrication of polymer nanocomposites with high mechanical performance that possess satisfactory electrical and thermal conductivities is desirable for engineering applications such as electrical conducting adhesives [9,10], flexible electronics [11,12], sensors and actuators [13,14], antistatic coatings [15–17], electromagnetic interference shielding materials [18–21], etc. Different nanofillers have been used to prepare nanocomposites with almost all types of polymers, such as thermoplastics, thermosets and elastomers that exhibit unusual property combinations and unique design possibilities [22–27,27–29]. Many products based on polymer nanocomposites have been already developed by proper selection of matrix, nanofiller, synthesis method and surface modification of either the nanofiller or polymer [15,17,19,26,27,27–31]. For the numerous general and industrial applications, the enhancements in thermal, electrical, and mechanical properties of nanocomposites have resulted in major interest [31–34]. The applications of high performance nanocomposites include: packaging, fuel cell, solar cell, fuel tank, plastic containers, power tool housing, and cover for portable electronic equipment such as mobile phones, etc. Generally, silicone, epoxy, acrylate and urethane based electrically conductive adhesive are popular for electronics applications such as EMI shielding or for antistatic systems [18–21]. Though epoxy is strong, it will crack on surfaces while urethane based adhesives offer high peel strength and flexibility. So, PU based

electrically conductive adhesive composites were prepared in this study to use in the structures that expand or contract with temperatures.

The conceptual structural unit of sp^2 hybridized carbon nanofillers includes a broad class of carbonaceous solids and primarily consist of elemental carbon bonded through sp^2-hybridization [35,36]. The sp^2 carbon nanofillers such as CNTs, carbon nanofibers (CNFs), and graphene have been used at lower weight percentages than the conventional fillers to create polymer composites with electrical conductivity without decreasing the mechanical properties [7,37]. In previous studies, highly suitable conditions for the transfer of either a mechanical load or an electrical charge from the individual nanotubes or graphene to the polymer composite have been sought after [37–39]. The basic conditions to obtain the desired properties of a nanofillers based composite is the efficient dispersion of the individual nanofillers and the establishment of strong affinity (covalent or non-covalent) of the nanofillers with the surrounding polymer matrix [40,41]. Among the various bonding types that are used for the functionalization of CNTs and graphene, covalent bonding is preferred because it provides the greatest stability and strongest coupling of the polymers to the nanotube walls and graphene surface [42,43]. The addition of the covalent bond on the carbon atom changes its hybridization from sp^2 to sp^3 and that disrupts or suppresses the electronic properties of nanotubes or nanosheets [38,39,44]. While the functionalization of CNTs or GNPs or CB by covalent and non-covalent bonding plays an important role for the dispersion of the nanofillers in the polymer matrices; there are two potential drawbacks to creating electrically conductive composites with nanofillers after their covalent functionalization. The first drawback is that the aspect ratios of the nanofillers decrease due to the rupture of nanofillers during modification. The second drawback is that the covalent grafting of any polymer or any functional groups on the surface of carbon nanofillers disturbs

the path for the flow of electrons [45]. The changes in the intrinsic conductivity of the carbon nanofillers directly influence the electrical conductivity of the composite created.

The nanofillers should be properly distributed in the polymer matrix to form an effective conductive path and the electrical resistances at nanofillers-polymer and/or at nanofillers-nanofiller interfaces must be minimized. The quality and the quantity of the nanofillers interconnection are very important for the preparation of the electrically conductive nanocomposites [37,39]. The fine dispersion of the carbon nanofillers in a viscous polyol liquid is a key factor for the preparation of the carbon nanofiller based PU nanocomposites with desirable properties. Non-polyol based methods such as, non-covalent stabilization of nanofillers in a solvent, are possible with the addition of a surfactant but are generally considered to be undesirable for the polymer nanocomposites in terms of the electrical and mechanical properties. Xia et al. [46] reported that ball milling can be used to break up agglomerates of CNT into polyol and thereby create a stable dispersion of the CNTs in polyol. Ultrasonication has been shown to be more effective than the use of simple stirring or ball milling for the preparation of metastable suspensions of CNTs or GNPs or CB/polymer mixtures without damaging the fillers [47],[48]. To overcome the problems associated with the dispersion of the pristine carbon nanofillers in the polymer matrix, we utilized a simple and an effective technique for the dispersion of the pristine carbon nanofillers in tetrahydrofuran (THF) by using a component of PU i.e. polyol (PTMEG1000) as stabilizer during sonication. The dispersion of the pristine carbon nanofillers (GNPs, CB and MWCNTs) in polyol was found to be agglomerate-free for CNTs and GNPs even after the removal of the THF.

Usually, the formation of the conductive networks of hybrid fillers in polymers can be controlled by adjusting filler concentrations and ratios to achieve the lowest percolation threshold. Araby et al. [49] developed the electrically conductive and mechanically strong

GNPs based styrene butadiene rubber (SBR) composites by a melt compounding method, where the electrical percolation threshold was achieved at 16.5 vol % GNPs loading. The GNPs used in their experiment were added without any interface modification and processed by industrial methods. Furthermore, they also observed the improvement of the Young's modulus and the tensile strength 560% and 230%, respectively with the addition of 24 vol% of the GNPs. Yuen et al. [50] reported the improvement of the tensile properties of CNTs/polyimide composites by using an acid-modified and an amine-modified multi-walled carbon nanotubes. In their study, the surface and volume electrical resistivity of unmodified CNTs/polyimide composites were lower than those of the modified CNTs/polyimide nanocomposite. It is obvious that the surface modification of CNTs by covalent bonds reduces the electrical conductivity due to disturbing the sp^2 hybrid carbon of CNT for delocalization of π-π electron. Li et al. [51] demonstrated a strongly aspect ratio dependent percolation threshold for the electrical conductivity of CNTs (3 wt %), CNFs 5 (wt %), GNPs (12 wt %) and CB (15 wt %) based poly(propylene) (PP) nanocomposite through a facile solution dispersion method, where CNTs and CNFs could form a filler network in the PP matrix at a lower loading than CB and GNPs. The morphological differences of the conductive networks depend on the nature of the fillers.

Lan et al. [52] showed facile fabrication technique of reduced graphene oxide (RGO) based PU/PP nanocomposites with high electrical conductivity and improved mechanical properties. They achieved very low percolation threshold (0.054 wt %) of RGO and favorable double percolation effect due to selective location of RGO in the PU phase. Wen et al. [53] studied the effect of CB and CNTs in PP for the electrical conductivity of composite and obtained highest efficient grape-cluster-like conductive network at a CB:CNTs weight ratio of 6. The percolation thresholds for CB/PP and CNTs/PP were 5.3 vol% and 3.2 vol% respectively; these values were decreased to 2.6 vol % for CNTs/CB/PU hybrid

nanocomposite. This is an indication of the synergism of CB and CNTs in PP for electrical conductivity. Oh et al. [54] reported enhanced electrical networks of polydimethylsiloxane nanocomposites via the use of a CNTs-graphene hybrid system. They noticed synergistic effects in the electrical conductivity in the CNT-graphene hybrid nanocomposite system by formation of 1D (CNTs) - 2D (graphene) interconnection [55]. Appel et al. [56] prepared the PU nanocomposites from a solvent-free dispersion of carbon nanofillers in polyol by an in-situ polymerization method. In their study, the maximum possible loading of carbon nanofillers CNTs, thermally reduced graphene oxide (TRGO) and CB was 2 wt % due to rapid increase of the viscosity of the composite before casting. Even though they increased the mechanical properties of PU after loading all carbon nanofillers, the value of electrical conductivity of all the nanocomposites were far below the percolation threshold. There are no reports that show the electrical conductivity of PU nanocomposites prepared by the solvent free bulk in-situ polymerization method till date in open literature.

In this study, we used single, binary and ternary carbon nanofillers in PU for the preparation of the electrically conductive and mechanically robust nanocomposites by the solvent free bulk in-situ polymerization. Instead of the chemical modification of the carbon nanofillers, an ultrasonication of the carbon nanofillers dispersion in tetrahydrofuran (THF) and polyol was employed, and the masterbatches of nanofillers in polyols was obtained after the removal of the solvent. The polyol prevented the re-agglomeration of the nanofillers and the stable dispersion of the nanofillers in polyol (5 phr) was achieved. The synergetic effect for the electrical properties of the PU nanocomposites was achieved at only 2 wt % loading of ternary hybrid fillers at definite weight ratio due to the different dispersion characteristics of the GNPs, CB, and MWCNTs in the polyol. Here, we achieved highest value of relaxation modulus and relaxation time of ternary carbon nanofillers based conductive PU

nanocomposite due to the obstruction of the movements of polymer chain segments by the hierarchical organization of the nanofillers.

2. Experimental

2.1. Materials

Natural graphite (NG) (98%, 50 mesh) was purchased from Hyundai Coma Ind. Co. Korea. Lithium metal (granule, 99.8%), naphthalene (99.8%), tetrahydrofuran (THF) (inhibitor free, HPLC grade) and tetra-ethylammoniumbromide (TEAB) all from Sigma-Aldrich were used for the intercalation of the NG. The MWCNTs used in this study were prepared by a chemical vapor deposition method (multi-walled CNTs, supplied by Iljin Nanotech Co., Ltd., Seoul, Korea). The diameter and length of CNTs range 10-30 nm and 10-50 μm, respectively, with an estimated aspect ratio of 500–5000. Conductive CB (Ketjenblack, EC-600JD) was used as another carbon nanofiller, which has a spherical shape with a diameter in the range of 20-60 nm. Poly(tetramethylene glycol) (PTMEG) (Average Mw = 1000 g/mol), 4,4'-methylene diphenyl diisocyanate (MDI), and 1,4-butanediol (BD) from Sigma-Aldrich were used for the in-situ polymerization of the PU nanocomposites.

2.2. Preparation of graphene nanoplatelets

Graphene nanoplatelets (GNPs) were synthesized from the natural graphite (NG) by our previously reported an ion-exchange induced intercalation and exfoliation method with minor modification [58,59]. Here, donor-type ternary graphite intercalation compounds (GICs) of natural graphite were formed with lithium ions and tetrahydrofuran (NG-Li-THF) then ion exchange was carried with tetra-ethyl ammonium cations to expand the interlayer distance. Typically, NG (10 g), lithium metal (1.16 g), tetrahydrofuran (THF) (50 ml) and naphthalene (17.7 g) were added in the three neck flask with continuous flush of nitrogen in the flask. Then, the flask was sealed with paraffin tape and carried out continuous magnetic stirring for 24 h at room temperature. The stoichiometric amount of TEAB was added in the above

mixture for ion-exchange induced intercalations and further agitated at room temperature for 24 h. The resulting product, GICs was washed with THF and dried at 70 ^{o}C in a conventional oven for 3 h. Then GICs (1 g) in quartz glass bowl was transferred into a microwave oven and treated for 1 min under the flow of nitrogen for the exfoliation into graphene nanosheets. The volumetric expansion ratio was measured at around 200 times. The cooled product was dispersed in 1% HCl solution and sonicated for 2 h and washed several times by using mixture of ethanol and acetone (1:1 by volume) and dried in the oven for 3 days at 90 ^{o}C.

2.4. Preparation of PU hybrid nanocomposites

The processing steps for the fabrication of the ternary hybrid nanocomposite is shown in Figure 1. First, masterbatches of carbon nanofillers in polyol (5 phr) were prepared separately by using ultrasonication. Sonication time was varied depending on the nature of carbon nanofillers. Typically, GNPs dispersion in THF (0.5 wt %) with polyol was prepared after sonication at 250 W for 12 h. The sonication time of CB and MWCNTs dispersion in THF with polyol was fixed 12 h and 7 h, respectively keeping all the other conditions same as GNPs. Then, the carbon nanofillers dispersion in polyol (5 phr) was obtained after the removal of THF by vacuum distillation at 60 ^{o}C. The masterbatches of carbon nanofillers in polyol was dried in a vacuum oven for 3 days at 90 ^{o}C. A hybrid of different fillers in polyol with desired concentration was prepared by mixing the masterbatches and dilution with neat polyol. Then, the composites of carbon nanofillers based PU prepolymer were prepared after the reaction of MDI with the carbon nanofillers dispersed polyol at 65 ^{o}C for 1 h. BD was added for chain extension and the mixture was casted in a preheated mold to cure at 120 ^{o}C for 24 h once a vacuum was used in order to remove any bubbles generated during stirring. The molar ratio of MDI, PTMEG, and BD was fixed 2:1:1 having HS content 37.1% for neat PU and nanocomposites preparation.

2.5. Characterization

Transmission electron microscopy (TEM; JSM-6400) was used to measure the morphology, thickness and size of GNPs, MWCNTs and CB. The pristine nanofillers in THF (0.5 wt %) were sonicated for 7 h and diluted to 0.01 mg/ml for TEM measurement. The masterbatches of carbon nanofillers in polyol was diluted 0.01 mg/ml with THF and copper grid was dipped 3 times and dried in oven at 70 ^{o}C for 3 h for TEM measurement. For the sample preparation of nanocomposite (GCM112-PU2), it was dissolved in DMF and mild sonicated for 10 min. The concentration was fixed 0.01 mg/ml for the preparation of all TEM samples. High resolution transmission electron microscopy (HRTEM; JEOL 2100 microscope, Japan) was performed at 200 kV for the determination of the thickness of GNPs. The nature of carbon nanomaterials especially the defect and order of graphitic layer were determined by Raman scattering (633 nm, neon laser). The electrical surface resistivity of nanocomposite films (thickness = 1.0 mm) was measured at room temperature using surface resistivity tester (Trustat ST-3 from SIMCO, Japan) [60]. The tester was just placed on the top of the PU composite film to measure its surface resistance. The measured values are the average of the three measurements. Mechanical strength of composites was measured by using a Universal Testing Machine (ASTM D 412-98a) at room temperature with a cross head speed of 500 mm/min. The slope of initial low strain region was used to determine the Young's modulus of neat PU and composites. The stress relaxation tests in a solid state of a neat PU and nanocomposites were proceed in a tensile mode on rectangular-shaped specimens at 30 and 50 ^{o}C, using dynamic mechanical analysis (DMA) Q800; from TA Instruments Inc., USA. The tensile strain applied was 20%, which was chosen based on the results of a static tensile test, and an equilibrium time was set 5 min for each temperature measurement. The microscopic features of nanocomposites were characterized by field emission scanning electron microscopy (FE-SEM Hitachi Co., Tokyo, Japan). The cryogenically fractured surface of the composite was coated with gold for FE-SEM measurement. The rheological

behaviors of the polyol and the masterbathes of carbon nanofillers (5 phr) in polyol were studied at 60 ^{o}C by a TA Instruments, AR 2000 Rheometer. The measurements were performed by employing a parallel plate rheometer during steady shear and in the oscillation shear mode. Stress relaxation of nanocomposites and neat PU in melt state (180 °C) was performed in an ETC Steel parallel plate (25 mm diameter of upper geometry) using the above same Rheometer. The test was performed under a nitrogen atmosphere with 10% strain of sample for 10 min. This strain value was chosen at the linear region after a series of tests.

3. Results and discussion

3.1. Rheological analysis of the masterbatches of carbon nanofillers in polyol

TEM image of GNPs shows thin folded multi layers of graphene sheets with lateral size ~5 μm on the TEM grid (Figure 2a). The HRTEM image of GNPs (Figure 2b) shows numerous graphitic layers at the edge having thickness ~8 nm [58]. The aggregated network structure of CB was observed in Figure 2c. Even after the sonication of MWCNTs in THF, agglomerated structure of CNTs were observed on the TEM grid (Figure 2d). We clearly observed the effect of the addition of polyol for the debundling of MWCNTs during the sonication of the mixture of CNTs and polyol in THF (Figure S-1b). The polyol prevented the reagglomeration of the MWCNTs even after the removal of solvent. We believed that the surface of MWCNTs absorbed the polyol that prevented the re-aggregation of nanotubes even after the removal of the solvent [48,61]. Similar phenomenon was observed for GNPs, where polyol absorbed on the surface of GNPs and prevented the re-stacking of GNPs sheets even after the removal of solvent (Figure S-1a). In the case of CB/polyol masterbatch, even the polyol was absorbed on the surface of CB as shown in TEM image (Figure S-1c), the agglomerated structure of CB was not broken completely even after 12 h sonication. Sonication time was fixed based on the several experiments for the effective dispersion of fillers. In case of CB, even more than 12 h sonication did not show significant differences. The hybrid of GNPs, CB

and CNTs at 1:1:2 ratio in polyol in Figure S-1d shows the network structure of three fillers in polyol, where well separated CNTs as well as small aggregates of CB and large thin flat surface of GNPs are embedded within the hybrid polyol mixture. Raman scattering spectroscopy is widely utilized for the characterization of carbon nanofillers and can explain in terms of D/G ratio and also by the 2D band shape, as shown in Figure 3. The prepared GNPs showed the D band at 1365 cm^{-1} and G band at 1613 cm^{-1} and the ratio is 0.78, which suggests that, even though the flake size is small, disorder in the sp^2 carbon lattice [59]. The intensity and the location of the 2D band are sensitive with the doping of the metals or interaction with the impurities. The shape of the 2D peak of GNPs in our work is changed, which might be due to the decreased size of the graphene flakes or edge doping. The strong intensity of D band of MWCNTs and CB indicates the disorderness of graphitic layers in both MWCNTs and CB.

Neat PU is electrically insulator and mechanically not strong enough for many engineering applications. Availability of the stable masterbatches of the carbon nanofillers in the polyol is desirable to prepare the mechanically robust and electrically conductive PU nanocomposites for many real world applications. Rheological study of the masterbathes of nanofillers in the polyol provides the information about the dispersion state and the agglomeration process of nanofillers in the polyol. Generally, the nature of nanofillers significantly affects the viscosities of masterbatches. It is expected that the strong interaction and the fine dispersion of the nanofillers in polymer enable the enhancement of viscosity [62,63]. As mentioned above, even the nanofillers are used without modification, the absorption of polyol on the surface of nanofillers made stable dispersion of nanofillers in polyol even after the removal of solvent [48,61]. Especially, debundalization of CNTs was found effective after sonication in THF in presence of polyol and prevented the reaggregation even after the removal of solvent. Similarly, sonication of GNPs dispersion in THF in

presence of polyol, exfoliates the GNPs into thinner layer and found stable dispersion after removing solvent. Furthermore, we observed stable masterbatches of CNTs and GNPs in polyol (PTMEG, Mw=1000) even after 6 months at room temperature. So, we felt the necessity of rheological characterization to know the structure of carbon nanofillers in the masterbarches of polyol. Figure 4a&b compares the viscosity curves of carbon nanofillers (5 phr) dispersion in polyol at 60 ^{o}C. Here, pure polyol (PTMEG 1000) shows Newtonian behavior with independence of a shear rate. The masterbatches of nanofillers dispersion in polyol shows shear thinning behavior with increasing the shear rate [60,64]. The strong shear thinning behavior of the carbon nanofillers in polyol is the indication of the network formation (Figure 4b) [65–67]. However, the nature of the viscosity curves of the different fillers in polyol is significantly different. At 5 phr GNPs in polyol, the increment of the viscosity is significantly higher than the neat polyol, but lowers than the 5 phr CNTs or CB dispersion in polyol. The Newtonian region disappears and the only shear thinning region remains throughout the entire shear rate for 5 phr CNTs and CB dispersion in polyol. The strong nanofiller-nanofiller interaction is responsible for the increase in shear viscosity without the Newtonian plateau region and play a dominant role in the rheological behavior of the nanocomposites [68]. The existence of yield stress in the all masterbatches is a sign of the strong particle-particle interactions [67]. In other words, non-interacting particle-filled systems do not show the yield stress. Furthermore, the nanotubes are entangled (knotted) at low shear stress and exhibit a solid-like behavior. Above a critical shear stress, they transform to a liquid-like state by dispersing the nanotubes that is clearly observed in 5 phr MWCNTs in PTMEG at 60 ^{o}C (Figure 4b). Moreover, at the first region of the viscosity curve of masterbatch of MWCNTs, the viscosity decreases by up to one decade with continuous decreasing the stress and then the stress remained approximately constant. The first region attributes a thixiotropic behavior due to the microstructural changes. Then, the value of shear

viscosity was decreased with increasing shear stress in the 2nd region without thixiotropic behavior. The viscosity curves of carbon nanofillers (5 phr) dispersion in polyol were also obtained at three different temperatures for the further understanding of the nanofiller-nanofiller interaction in polyol (Figure S-2). The synergistic effect of hybrid fillers was clearly reflected in the viscosity curves of GCM112-polyol at 80 ºC, 60 ºC and 40 ºC (Figure S-2d). The storage modulus (*G*') and the loss modulus (*G*'') from the dynamic frequency scan measurements for the masterbatches of the carbon nanomaterials in polyol (5 phr) are compared in Figure 4(c) and (d) respectively. Figure 4(c) shows the effect of the carbon nanomaterials on *G*' of masterbatches, in which the magnitude of *G*' for GNPs is nearly one order magnitude lower than CNTs, CB and ternary hybrid fillers (GCM112). For the masterbatch of 5 phr GNPs in polyol, the degree of dependence of low-frequency *G*' on the frequency, ω, reflects the sensitivity of GNPs on the viscoelastic properties. With 5 phr loading of the CNTs and CB in polyol may already experience the solid-like viscoelastic response results from the formation of percolated network [66]. The unique behavior of the masterbatch of GNPs in polyol than the other masterbatches might be due to the GNP-polyol interlayer slipperiness caused by the low surface friction of graphite [51]. We observed the frequency dependent behavior for the *G*''curves of all masterbatches in Figure 4(d).

3.2. Electrical, thermal and mechanical properties of PU hybrid nanocomposites

Preparation of single or binary carbon nanofillers based PU nanocomposite by a solvent free bulk in-situ polymerization can improve the mechanical properties of nanocomposite significantly due to the fine dispersion of fillers in the PU matrix. But, the primary conductive networks of fillers are broken during processing of the PU nanocomposites by the solvent free bulk in-situ polymerization through prepolymer method; as a result the surface resistivity of composite was observed high [59]. In this study, PU nanocomposites were

prepared via solvent free bulk in-situ polymerization, where re-agglomeration of carbon nanofillers was not possible due to the solidification of PU within 2-3 min of chain extension. Furthermore, there are some limitations to prepare large content of the carbon nanofillers based conductive PU composites by solvent free bulk in-situ polymerization. Even we proceeded the experiment with the maximum possible loading of nanofillers such as GNPs (5 wt %), MWCNTs (2 wt %) and CB (3 wt %) in PU by solvent free bulk in-situ polymerization, a surface resistivity of PU composite was not decreased significantly (Table 1). Due to the elastomeric nature of PU, it often has far higher percolation thresholds for the electrical conductivity than the other polymers [49].

In MWCNTs/PU composite (2 wt %), even the primary networks are broken during processing; long length (~20 μm) with high aspect ratio of MWCNTs are able to form the secondary networks by the contact of the end of MWCNTs for electrical conductivity in the range of hopping or tunneling distance. The synergistic effect can generate from the combination of two or more conducting fillers with unique geometric shapes and aspect ratios as well as different dispersion characteristics in polymer [53,54,69,70]. Ma et al.[71] reported the remarkable enhancement of the electric conductivity of the epoxy matrix with the addition of CNTs into the composites filled with CB, where the CB nanoparticles were filled between the gap of CNTs, and the conductive networks were generated. In our study, a new strategy was designed to improve the electrical and mechanical properties of PU composites by the incorporation of hybrid of 0-D CB, 2-D GNPs, and 1-D MWCNTs for lowering the cost of the final product. Here, the long and twisted MWCNTs can bridge adjacent GNPs and inhibit their aggregation, while the grape-like CB aggregates enriched around the junction of MWCNTs and GNPs resulting in an increased contact surface area among the carbon structures in the polymer for the formation of the hierarchical carbon conductive networks. The optimum ratio of the three fillers CB, MWCNTs and GNPs in PU for the electrical and mechanical properties

was found based on the several experiments. The sample codes and the electrical surface resistivity of the different composites are presented in Table 1. Except CNT-PU2, all the nanocomposites containing single and binary carbon nanofillers showed very high surface resistivity. Generally, we can expect that the addition of the hybrid of GNPs and CB or GNPs and MWCNTs in PU should show synergistic effect [53,54,69,70] for the electrical conductivity than the single filler loading in PU, but in this study, electrical conductivity was not achieved at total 2 wt % loading of binary hybrid filler with different ratios in PU. Furthermore, the preparation of the series of the composites containing more than 2 wt % of the hybrid filler was not possible due to the high viscosity of the composite before casting by the solvent free bulk in-situ polymerization. For the ternary hybrid filler loading, interestingly, only 1:1:2 and 1:1:3 ratios of GNPs, CB and MWCNTs showed the improvement of the electrical properties of the 2 wt % PU composite, while 1:1:1 and 2:1:1 and 1:2:1 ratios of GNPs, CB and MWCNTs in PU has an insulating property. From the above results, it can be understood that the formation of the hierarchical conductive networks is dominated by the MWCNTs with their high aspect ratio. The amount of MWCNTs content is only 0.66, 0.5 and 0.5 wt % in GCM111-PU2, GCM211-PU2, and GCM121-PU2 respectively, which is not enough to form the bridge among the GNPs with CB for the formation of the hierarchical conductive networks. Figure 5 shows the electrical surface resistivity versus a fix content (2 wt %) of different carbon nanofillers in single, binary and ternary forms, where the improvement of the electrical properties was noticed only for CNT-PU2 and GCM112-PU2. Furthermore, it was not possible to prepare a series of more than 2 wt. % ternary hybrid composites due to a very high viscosity of the composite after chain extension with BD. The effect of single, binary, and ternary carbon nanofillers on the degradation of polyurethane nanocomposite was compared using TGA thermograms (Figure S-3). It is worth to note that first step degradation of the hard segment of PU in the all composites was found slightly earlier

temperature than neat PU. But, the degradation temperature of the soft segment (second step degradation) was found at higher temperature than neat PU. Specially, the second step degradation temperature of ternary hybrid composite, GCM112-PU2 was observed significantly higher temperature than other composite and also the ash content was found nearly 20%. Figure S-4 displays the Raman scattering spectra of neat PU and carbon nanomaterials/PU composites. Neat PU shows strong peaks at 1180, 1251 and 1308 cm^{-1} (urethane amide I, II and III), 1433 cm^{-1}[υ_{sym}(Ar) and urethane amide] and 1612 cm^{-1} υ_{sym}(Ar).[48] Based on the nature of the carbon nanofillers in PU, characteristic differences on the position and intensity of D-band and G-band of nanocomposites were clearly observed. Along with the characteristic peaks associated with neat PU, D-band and G-bands are clearly observed in GNP-PU2. However, the D/G ratio was changed from 0.78 (GNPs) to 0.63 (GNP-PU2), which was the evidence of the further exfoliation of GNPs into thin sheet during sonication with THF and polyol. Raman scattering spectra of CB-PU2 shows strong broad peak of the D-band at 1311 cm^{-1}; and G-band was masked with 1612cm^{-1} υ_{sym}(Ar) of PU. In CNT-PU2, G-band was observed with the fusion with 1612cm^{-1} υ_{sym}(Ar) of PU with some broadening. The presence of all three nanofillers in PU is reflected on the Raman scattering spectra of GCM112-PU2, where the D/G ratio was 0.79 and the nature of D and G bands indicates the mixture effect of three fillers. Generally, increasing disorder in graphitic fillers broadens D and G bands, and the relative intensity of D band increases [72]. An FT-IR spectroscopy was performed to know the extent of inter-urethane hydrogen bonding interaction in the neat PU and hybrid nanocomposites (Fig. S-5). Neat PU as well as all the nanocomposites have two distinguished bands: at 1731 and 1702 cm^{-1}. The peak at 1731 cm^{-1} is associated with -C=O groups that are ‘‘free’’ (non-hydrogen bonded) and the peak at 1702 cm^{-1} resulted from a hydrogen bonding with urethane N-H groups. At 2 wt% loading of all carbon nanomaterials in PU, the intensity ratio between hydrogen-bonded and ‘‘free’’ carbonyl domain was

decreased from 1.107 (Neat PU) to 1.07 (GNP-PU2), 1.09 (CB-PU2), CNT-PU2 (1.07), GNP-CB-PU2 (1.09) and GCM112-PU2 (1.06), respectively that was inferred from the decrease peak intensity at 1702 cm^{-1}[73]. The insertion of the carbon nanofillers in the hard domain of PU suppresses the hydrogen bonding in HS and enhances the phase mixing in PU. Even the phase mixing was observed in composites, the mechanical properties of composites were improved efficiently by the fine dispersion of nanofillers [74].

Tensile test was performed to investigate the effect of carbon nanomaterials as a reinforcing phase in the polyurethane nanocomposites. Tensile strength and Young's modulus of the nanocomposites after the introduction of carbon nanomaterials in PU are summarized in Table 1. Pure PU shows a stress-strain curve with low value of Young's modulus. Significant improvement of Young's modulus was achieved with the addition of all carbon nanomaterials in PU. The effect of 2 wt % carbon nanomaterials on the tensile properties of PU nanocomposites is shown in Figure 6. Among the 2 wt % of single carbon nanomaterials based PU composite, MWCNTs showed the best performance for the improvement of the modulus and tensile strength. Although the tensile strength of CNT-PU2 composite was slightly higher than the neat PU, the Young's modulus of neat PU (11.92 MPa) was increased more than 2-fold with the 2 wt % CNT addition, CNT-PU2 (26.02 MPa). Furthermore, all the single-nanofiller-containing composites showed an improvement of Young's modulus more than 100%.

The debundalization of MWCNTs during sonication in THF and polyol mixture is effective to obtain finely dispersed nanocomposite, which is effective for the improvement of mechanical properties of nanocomposites. Even the slight aggregation and entanglement of 2 wt % MWCNTs in PU was ensued, elongation at break of composite is still near to neat PU. Previous reports show that addition of MWCNTs more than 0.5 wt % decreases the fracture strength of PU due to strong tendency of MWCNTs agglomeration [75,76]. Our results show

that even 2 wt % MWCNTs has higher tensile strength than the neat PU due to effective dispersion of MWCNTs with polyol. The strong increase in the elastic modulus of PU with MWCNTs addition is related to stiff MWCNT and MWCNTs interaction with the polymer. Molecular dynamics simulations showed that MWCNTs limit the configurational states of polymer chains; thus, increase stiffness [75]. A decrease in strength with the addition of GNPs was observed up to 5 wt % GNPs, which was expected due to limited effectiveness of load transfer from GNPs to PU. GNP diameter should be more than ~30 μm for effective strengthening, but our GNPs diameter was ~5μm, which limited the load transfer from PU to GNP according to shear-lag theory [77]. Nonetheless, GNPs and CB based PU composites (2 wt %) had higher elongation at break than the neat PU. These results suggest that the GNPs, CB and CNTs preferentially affect the hard microdomains rather than the soft segments of PU to keep the large strain-to-failure of the polyurethane nanocomposites [64].

Furthermore, the binary hybrid nanofillers showed the better improvement of tensile strength and Young's modulus than the average value of two corresponding single filler loading at 2.0 wt %, which is the indication of the synergistic effect for the mechanical reinforcement in hybrid nanocomposites (Table 1)[54,59,70,71,78]. In GCM112-PU2, the three fillers of different dimensions are finely dispersed in the PU matrix and perform as a single filler with high aspect ratio and show the synergetic effect for the improvement of mechanical properties [54,71]. Although numerical studies reveal the origins of strengthening and stiffening in polymer nanocomposites containing single-type fillers [79]. High-fidelity simulations are required to identify and quantify synergistic mechanical enhancement in three-filler-containing nanocomposites.

3.3. Hierarchical conductive network structure in the hybrid nanocomposite

The degree of the carbon nanofillers dispersion in the PU matrix primarily determines the nanofillers reinforcing efficiency, which can directly evaluate by the morphological

characterization. Figure 7a-f shows the representative FESEM images of the polymer composites with 2.0 wt % different carbon nanofillers. For the GNPs (Figure 7a) and CB (Figure 7b) nanocomposites, both GNPs sheets and CB nanoparticles were isolated and formed islands other than the network paths in the matrix and expected that both should have high surface resistivity in this dispersion state. Furthermore, the spherical geometry of CB particles has tendency to form agglomerates easily and did not disperse uniformly in the PU matrix and part of them tended to form aggregates in certain regions (Figure 7b). Even the exfoliation of GNPs occurred by the application of ultrasonication; agglomeration and bending also happened in the GNPs system depending on the processing condition (Figure 7a), which leads to limited exploitation of the high aspect ratio property [80].

As shown in Figure 7c, it is clear that the dispersion of MWCNTs in the PU matrix is more uniform than CB and GNPs dispersion. At 2 wt % loading of MWCNTs in PU, the electron conduction path was formed. In certain areas, the MWCNTs clusters appeared and some MWCNTs were entangled, which are attributed to the strong intermolecular forces among MWCNTs and interfacial interactions between the MWCNTs and the PU matrix. At 2 wt % loading of binary fillers MWCNTs and GNPs based PU composite (Figure 7d), conductive networks were not formed due to aggregation of GNPs and insufficient bridging of MWCNTs between graphene sheets. Specially, in the ternary hybrid system GCM112-PU2 (Figure 7e,f), addition of 0.5 wt % CB prevented the aggregation of GNPs (0.5 wt %) and hierarchical conductive network was constructed by bridging with 1 wt % of MWCNTs. The above results show that the influence of MWCNTs on the properties of PU composites is different with CB and GNPs, which can be ascribed to the structure and aspect ratio difference among them. Figure 7g,h shows TEM micrographs of the GCM112-PU2 nanocomposite, where the conductive networks are formed by the combination of MWCNTs, GNPs and CB. Well separated MWCNTs from the bundle of MWCNTs are observed in TEM

images of GCM112-PU2. Furthermore, small clusters of CB were seen at the junction of MWCNTs and GNPs (Figure 7h) for the hierarchical conductive network formation in the ternary hybrid filler system.

3.4. Understanding the relationship between stress relaxation behavior and conductive network structure of carbon nanomaterials in the hybrid PU composites

Stress relaxation is a well-known phenomenon in a thermoplastic polymer in which a sample is very quickly distorted to a set length, and the decay of the stress exerted by the sample as a function of time is measured [46,81–88]. In our knowledge, there are not any studies on the stress relaxation behavior of carbon nanofillers based PU nanocomposites. The role of nanofillers' structure, morphology, and networking in polymer composite on the relaxation behavior is not well explored and the relaxation mechanisms are not fully understood yet. The main objective of the present study is to investigate the relaxation behavior of carbon nanofillers filled PU with special reference to particle size and aspect ratio, filler morphology, filler loading to understand the conductive network formation of filler in the PU matrix. The presence of carbon nanofillers in PU leads to the formation of a significant interphase zone with changed polymer mobility, namely chain immobilization, which results in the enhancement of stress relaxation of composite [85–87]. Good nanofillers–matrix interfacial bonding further increases relaxation modulus and relaxation time through frustrating chain disentanglement, stretching and fragmentation of the macromolecule.

Figure 8a presents the schematic diagram of the stress relaxation test, where single strain 10% was employed for the measurement. Figure 8b shows the effect of nanofillers on the stress relaxation modulus of nanocomposites at melt state (180 ^{o}C) by using Rheometer. The presence of nanofillers in polymer can enhance the viscosity of reaction system,

changing molecule diffusion ability. In this study, all the pristine nanofillers were used without any surface modification, so, the final dispersion and distribution of nanofillers is dominant on the relaxation modulus of nanocomposites without any effect of cross-linking between PU matrix and carbon nanofillers. The plot of the stress relaxation time (calculated) and surface resistivity of PU nanocomposites is shown in Figure 9. The network structure of carbon nanofillers largely affected the confinement of the PU chain as a result electrically insulating nanocomposites (CB-PU2 and GNP-CB-PU2) exhibited small value of stress relaxation time than electrically conductive nanocomposites (CNT-PU2 and GCM112-PU2). Furthermore, the addition of three different dimensional carbon nanofillers in GCM112-PU2 with fine dispersion constructs the conductive networks and decreases the mobility of the system i.e. slow down the movement of molecular segment. As mentioned above, the conductive network structure in GCM112-PU2 was formed by the combination of three different dimensional fillers in PU matrix where MWCNTs served as bridges among the GNPs and grape-like CB aggregates enriched around the junction of MWCNTs and GNPs. Even the short conductive channels are formed in GCM112-PU2 than CNT-PU2, the easy broken of the network structures in hybrid composite at melt state (180 ^{o}C) than only MWCNTs entanglement in CNT-PU2 results the values of the stress relaxation modulus and relaxation time in GCM112-PU2 were lower than CNT-PU2. Figure 10 displays the effect of nanofillers on the stress relaxation modulus of nanocomposites at very far below the melting point of PU nanocomposite viz. at 30 ^{o}C and 50 ^{o}C by using dynamic mechanical analysis. Interestingly, the relaxation modulus and relaxation time of GCM112-PU2 composite were observed higher than CNT-PU2 composite in the solid state of composite by performing stress relaxation test using dynamic mechanical analysis. It is due to the fact that the network of the three conductive nanofillers in PU in the solid state are strong enough, which can obstruct the movements of polymer chain segments and restrain the relaxations of chain (Fig.

S-6). Therefore, the relaxation modulus of GCM112-PU2 is higher than CNT-PU2 composite. Finally, relaxation time and modulus of both conductive nanocomposites CNT-PU2 and GCM112-PU2 are significantly higher than that of the insulating polymer nanocomposite such as CB-PU2 and GNP-CB-PU2 both in solid and melt state due to obstruction and slow down the movement of molecular segment [87].

In this study, modified Kohlrausch–Williams–Watt (KWW) equation [85,86] for single stretched exponential function was used to fit the stress relaxation curves.

$\sigma(t) = (\sigma_{max}-\sigma_{min}) \exp(-t/\tau)^{\beta} + \sigma_{min}$ ……(1)

Where t is the decay time in the relaxation test, $\sigma(t)$ is the relaxation stress at time t, σ_{max} is the unrelaxed stress at t=0, σ_{min} is the final time recorded stress at t~infinity and τ is the characteristic relaxation time. The stretching parameter β in equation (1) determines the narrowness of the distribution ($0<\beta\leq 1$), which is ~0.6 for flexible and isotropic polymers.

Time dependent relaxation modulus, E(t) and related form of the KWW equation are shown as follows

$E(t) = \sigma(t)/\varepsilon_o$ ……(2)

$E(t) = (E_0-E_f) \exp(-t/\tau)^{\beta}+E_f$ ……..(3)

Where E_0 is the unrelaxed modulus i.e. instantaneous modulus E(t=0), E_f is the long time relaxed modulus i.e. Ef ($t= t_f$), t_f is the final time recorded in stress relaxation test. Equation (3) can rearrange to obtain equation (4), which is useful to calculate the β and τ.

$\ln \ln [1/R(t)] = \beta \ln (t/\tau)$ ……(4)

Where R(t) is relaxation function and R(t) = E(t)- E(f)/(Eo - Ef).

The linear plot of ln ln [1/R(t)] vs ln(t) is shown in Figure S-7, where the slope as β and a y-intercept as $-\beta \ln\tau$. The value of β indicates the degrees of molecular mobility in polymer chains and inversely relates to the width of the relaxation spectrum. When β is closer to 0, it indicates a relatively large number of individual processes or a high degree of cooperativity

in the relaxation process. There is only one relaxation process at the extreme case of β=1 with the narrowest spectrum [85,86]. In our study, neat PU and all composites showed β =0.7±0.05, which lies within the range of elastomeric materials, affirming the validity of this model. Furthermore, β value of single filler and binary filler filled composites as well as neat PU showed in the range of 0.66 to 0.68, but GCM112-PU2 showed significantly high value ~0.75 due to narrowest relaxation time distribution compared with the neat PU and other composites. Figure 11 shows the plot of stress relaxation time at 50 ^{o}C versus surface resistivity of different types of carbon nanomaterials based PU nanocomposites.

It is clear that surface resistivity of carbon nanofillers/PU composites decreases with increasing the relaxation time of that nanocomposite. Here, the sample of lowest surface resistivity (GCM112-PU2) shows the longest relaxation time than the other nanocomposites. This is due to the restriction of the movement of molecular segments of PU by the network structure formed by the combination of three different carbon nanomaterials in GCM112-PU2. Finally, we propose the structure of different types of 2 wt % carbon nanofillers based PU composites as shown in Figure 11 (right). It is postulated that the conductive networks are broken during the preparation of GNPs/PU prepolymer and chain extension with BD (Figure 11a). The re-agglomeration of filler was not possible due to the high viscosity of prepolymer composite after chain extension with BD. In CNTs/PU composite (Figure 11b), even the primary conductive networks are broken during the processing, large length (~ 20 μm) with high aspect ratio of CNTs is able to form the network by the contact of the end of CNTs for electrical conductivity in the range of hopping or tunneling distance. In CB/PU (Figure 11c), not only the low aspect ratio of CB, but also the relatively poor dispersion of CB than other fillers in PU matrix also affected for the lower surface resistivity. For GCM112-PU2 composite, synergetic effect of three fillers was observed, when the CB occupied on the dead network of MWCNTs and GNPs; with enough MWCNTs for bridging among the GNPs

(Figure 11d). Here, the formation of hierarchical carbon network structure was effective to reduce surface resistivity in the hybrid PU nanocomposite.

4. CONCLUSIONS

The synergy arising from the combination of three conducting carbon nanomaterials with unique geometric shapes and aspect ratios as well as different dispersion characteristics in nanocomposite of PU has been demonstrated first time. In CNT-PU2 composite, even the primary networks are broken during the processing; large length (~ 20 μm) with high aspect ratio of MWCNTs is able to form the conductive network by the contact of the end point of CNTs in the range of hopping or tunneling distance and surface resistivity was reached $10^{8.6}$ ohm/sq. The low aspect ratio of CB and the relatively poor dispersion of CB than other fillers in PU matrix are responsible for the high surface resistivity of CB-PU2 composite ($10^{11.9}$ ohm/sq). In GNP-PU2, the formation of islands other than the network paths in the matrix depending on the processing condition limited the exploitation of the high aspect ratio property of GNPs and expected high surface resistivity ($10^{11.5}$ ohm/sq). Synergetic effect of three fillers for conductive network formation in GCM112-PU2 and GCM113-PU2 was possible by the extension of CNTs between the large flat surface area of GNPs, and the aggregation of CB at the junction of CNTs and GNPs largely reduced the surface resistivity ~ $10^{6.9}$ ohm/sq. On the other hand, the amount of CNTs content was not enough in GCM111, GCM211, and GCM121 to form the bridge among the GNPs with CB for the formation of conductive network. As a result, even the same amount of the total content of nanofillers, different ratio of hybrid fillers showed different electrical properties. The effect of ultrasonication for the exfoliation of carbon nanomaterials was evaluated by rheological measurement of masterbatches of carbon nanomaterials in polyol. The observation of the strong shear thinning behavior of the masterbatches of carbon nanofillers in polyol with

increasing shear stress is the indication of the network formation of fillers due to the strong particle-particle interactions. Even the particle-particle interaction was noticed in the masterbatches of carbon nanofillers in polyol; our method for the preparation of nanocomposite is solvent free bulk in-situ polymerization, where re-agglomeration of carbon nanofillers was not possible due to solidification of PU within 2-3 min of chain extension. The fine dispersion and conductive networks formation of nanofillers in PU decreases the mobility of the system i.e. slow down the movement of molecular segment in nanocomposites; as a result stress relaxation modulus and relaxation time were increased for conductive composites than insulating composites. Finally, in GCM112-PU2, the three fillers of different dimensions are finely dispersed in the PU matrix and they perform as a single hierarchical filler with high aspect ratio for the improvement of electrical, thermal, and mechanical properties.

Acknowledgements

P. Pokharel and D. Xiao acknowledge the grant support from Higasket Plastic Group Co. Ltd on completing this work.

References

[1] Oh JY, Jun GH, Jin S, Ryu HJ, Hong SH. Enhanced Electrical Networks of Stretchable Conductors with Small Fraction of Carbon Nanotube/Graphene Hybrid Fillers. ACS Appl Mater Interfaces 2016;8:3319–25. doi:10.1021/acsami.5b11205.

[2] Tan QC, Shanks RA, Hui D, Kong I. Functionalised graphene-multiwalled carbon nanotube hybrid poly(styrene- b -butadiene- b -styrene) nanocomposites. Compos Part B Eng 2016;90:315–25. doi:10.1016/j.compositesb.2015.12.020.

[3] Ramesh S, Khandelwal S, Rhee KY, Hui D. Synergistic effect of reduced graphene oxide, CNT and metal oxides on cellulose matrix for supercapacitor applications. Compos Part B Eng 2018;138:45–54. doi:10.1016/j.compositesb.2017.11.024.

[4] Verma M, Chauhan SS, Dhawan SK, Choudhary V. Graphene nanoplatelets/carbon nanotubes/polyurethane composites as efficient shield against electromagnetic polluting radiations. Compos Part B Eng 2017;120:118–27. doi:10.1016/j.compositesb.2017.03.068.

[5] Lau AK-T, Hui D. The revolutionary creation of new advanced materials—carbon nanotube composites. Compos Part B Eng 2002;33:263–77. doi:10.1016/S1359-8368(02)00012-4.

[6] Meincke O, Kaempfer D, Weickmann H, Friedrich C, Vathauer M, Warth H. Mechanical properties and electrical conductivity of carbon-nanotube filled polyamide-6 and its blends with acrylonitrile/butadiene/styrene. Polymer (Guildf) 2004;45:739–48. doi:10.1016/j.polymer.2003.12.013.

[7] Spitalsky Z, Tasis D, Papagelis K, Galiotis C. Carbon nanotube-polymer composites: Chemistry, processing, mechanical and electrical properties. Prog Polym Sci 2010;35:357–401. doi:10.1016/j.progpolymsci.2009.09.003.

[8] Li J, Sham ML, Kim JK, Marom G. Morphology and properties of UV/ozone treated

graphite nanoplatelet/epoxy nanocomposites. Compos Sci Technol 2007;67:296–305. doi:10.1016/j.compscitech.2006.08.009.

[9] Bittolo Bon S, Valentini L, Kenny JM, Peponi L, Verdejo R, Lopez-Manchado MA. Electrodeposition of transparent and conducting graphene/carbon nanotube thin films. Phys Status Solidi 2010;207:2461–6. doi:10.1002/pssa.201026138.

[10] Pu N-W, Peng Y-Y, Wang P-C, Chen C-Y, Shi J-N, Liu Y-M, et al. Application of nitrogen-doped graphene nanosheets in electrically conductive adhesives. Carbon N Y 2014;67:449–56. doi:10.1016/j.carbon.2013.10.017.

[11] Liu L, Weng W, Zhang J, Cheng X, Liu N, Yang J, et al. Flexible supercapacitor with a record high areal specific capacitance based on a tuned porous fabric. J Mater Chem A 2016;4:12981–6. doi:10.1039/C6TA04911G.

[12] Bora A, Mohan K, Doley S, Dolui SK. Flexible Asymmetric Supercapacitor Based on Functionalized Reduced Graphene Oxide Aerogels with Wide Working Potential Window. ACS Appl Mater Interfaces 2018;10:7996–8009. doi:10.1021/acsami.7b18610.

[13] Fowler JD, Allen MJ, Tung VC, Yang Y, Kaner RB, Weiller BH. Practical Chemical Sensors from Chemically Derived Graphene. ACS Nano 2009;3:301–6. doi:10.1021/nn800593m.

[14] Li C, Thostenson ET, Chou TW. Sensors and actuators based on carbon nanotubes and their composites: A review. Compos Sci Technol 2008;68:1227–49. doi:10.1016/j.compscitech.2008.01.006.

[15] Li C, Liang T, Lu W, Tang C, Hu X, Cao M, et al. Improving the antistatic ability of polypropylene fibers by inner antistatic agent filled with carbon nanotubes. Compos Sci Technol 2004;64:2089–96. doi:10.1016/j.compscitech.2004.03.010.

[16] Sangermano M, Pegel S, Pötschke P, Voit B. Antistatic Epoxy Coatings With Carbon

Nanotubes Obtained by Cationic Photopolymerization. Macromol Rapid Commun 2008;29:396–400. doi:10.1002/marc.200700720.

[17] Soto-Oviedo MA, Araújo OA, Faez R, Rezende MC, De Paoli M-A. Antistatic coating and electromagnetic shielding properties of a hybrid material based on polyaniline/organoclay nanocomposite and EPDM rubber. Synth Met 2006;156:1249–55. doi:10.1016/j.synthmet.2006.09.003.

[18] Wu N, Liu C, Xu D, Liu J, Liu W, Shao Q, et al. Enhanced Electromagnetic Wave Absorption of Three-Dimensional Porous Fe 3 O 4 /C Composite Flowers. ACS Sustain Chem Eng 2018;6:12471–80. doi:org/10.1016/j.carbon.2018.08.014.

[19] Zicheng Wang, Renbo Wei, Junwei Gu, Hu Liu, Chuntai Liu, Chunjia Luo, Jie Kong, Qian Shao, Ning Wang, Zhanhu Guo XL. Ultralight, highly compressible and fire-retardant graphene aerogel with self-adjustable electromagnetic wave absorption, Carbon. Carbon N Y 2018;139:1126–35. doi:https://doi.org/10.1016/j.carbon.2018.08.014.

[20] Zhang K, Li G-H, Feng L-M, Wang N, Guo J, Sun K, et al. Ultralow percolation threshold and enhanced electromagnetic interference shielding in poly(<scp>l</scp> -lactide)/multi-walled carbon nanotube nanocomposites with electrically conductive segregated networks. J Mater Chem C 2017;5:9359–69. doi:10.1039/C7TC02948A.

[21] Zicheng Wang, Renbo Wei, Junwei Gu, Hu Liu, Chuntai Liu, Chunjia Luo, Jie Kong, Qian Shao, Ning Wang, Zhanhu Guo XL. Ultralight, highly compressible and fire-retardant graphene aerogel with self-adjustable electromagnetic wave absorption. Carbon N Y 2018;139:1126–35. doi:https://doi.org/10.1016/j.carbon.2018.08.014.

[22] Li Y, Jing T, Xu G, Tian J, Dong M, Shao Q, et al. 3-D magnetic graphene oxide-magnetite poly(vinyl alcohol) nanocomposite substrates for immobilizing enzyme. Polym (United Kingdom) 2018;149:13–22. doi:10.1016/j.polymer.2018.06.046.

[23] Sun K, Xie P, Wang Z, Su T, Shao Q, Ryu JE, et al. Flexible polydimethylsiloxane/multi-walled carbon nanotubes membranous metacomposites with negative permittivity. Polym (United Kingdom) 2017;125:50–7. doi:10.1016/j.polymer.2017.07.083.

[24] Cui X, Zhu G, Pan Y, Shao Q, Zhao C (xinxin), Dong M, et al. Polydimethylsiloxane-titania nanocomposite coating: Fabrication and corrosion resistance. Polym (United Kingdom) 2018;138:203–10. doi:10.1016/j.polymer.2018.01.063.

[25] Cheng C, Fan R, Wang Z, Shao Q, Guo X, Xie P, et al. Tunable and weakly negative permittivity in carbon/silicon nitride composites with different carbonizing temperatures. Carbon N Y 2017;125:103–12. doi:10.1016/j.carbon.2017.09.037.

[26] Xu M, Ma K, Jiang D, Zhang J, Zhao M, Guo X, et al. Hexa-[4-(glycidyloxycarbonyl) phenoxy]cyclotriphosphazene chain extender for preparing high-performance flame retardant polyamide 6 composites. Polym (United Kingdom) 2018;146:63–72. doi:10.1016/j.polymer.2018.05.018.

[27] Wu Z, Cui H, Chen L, Jiang D, Weng L, Ma Y, et al. Interfacially reinforced unsaturated polyester carbon fiber composites with a vinyl ester-carbon nanotubes sizing agent. Compos Sci Technol 2018;164:195–203. doi:10.1016/j.compscitech.2018.05.051.

[28] Zhou B, Li Y, Zheng G, Dai K, Liu C, Ma Y, et al. Continuously fabricated transparent conductive polycarbonate/carbon nanotube nanocomposite films for switchable thermochromic applications. J Mater Chem C 2018;6:8360–71. doi:10.1039/C8TC01779D.

[29] Guo Y, Xu G, Yang X, Ruan K, Ma T, Zhang Q, et al. Significantly enhanced and precisely modeled thermal conductivity in polyimide nanocomposites with chemically modified graphene via in situ polymerization and electrospinning-hot press

technology. J Mater Chem C 2018;6:3004–15. doi:10.1039/C8TC00452H.

[30] Jiang W, Yu D, Zhang Q, Goh K, Wei L, Yong Y, et al. Ternary Hybrids of Amorphous Nickel Hydroxide-Carbon Nanotube-Conducting Polymer for Supercapacitors with High Energy Density, Excellent Rate Capability, and Long Cycle Life. Adv Funct Mater 2015;25:1063–73. doi:10.1002/adfm.201403354.

[31] Zhao M, Meng L, Ma L, Ma L, Yang X, Huang Y, et al. Layer-by-layer grafting CNTs onto carbon fibers surface for enhancing the interfacial properties of epoxy resin composites. Compos Sci Technol 2018;154:28–36. doi:10.1016/j.compscitech.2017.11.002.

[32] He Y, Yang S, Liu H, Shao Q, Chen Q, Lu C, et al. Reinforced carbon fiber laminates with oriented carbon nanotube epoxy nanocomposites: Magnetic field assisted alignment and cryogenic temperature mechanical properties. J Colloid Interface Sci 2018;517:40–51. doi:10.1016/j.jcis.2018.01.087.

[33] Wang C, Zhao M, Li J, Yu J, Sun S, Ge S, et al. Silver nanoparticles/graphene oxide decorated carbon fiber synergistic reinforcement in epoxy-based composites. Polym (United Kingdom) 2017;131:263–71. doi:10.1016/j.polymer.2017.10.049.

[34] Hu Z, Zhang D, Lu F, Yuan W, Xu X, Zhang Q, et al. Multistimuli-Responsive Intrinsic Self-Healing Epoxy Resin Constructed by Host–Guest Interactions. Macromolecules 2018;51:5294–303. doi:10.1021/acs.macromol.8b01124.

[35] Bianco A, Cheng HM, Enoki T, Gogotsi Y, Hurt RH, Koratkar N, et al. All in the graphene family - A recommended nomenclature for two-dimensional carbon materials. Carbon N Y 2013;65:1–6. doi:10.1016/j.carbon.2013.08.038.

[36] M. Pérez-Cadenas AG-RAE-ADC-TVM-A. Effect of surface, structural and textural properties of graphenic materials over cooperative and synergetic adsorptions of two chloroaromatic compounds from aqueous solution. Catal Today 2018;301:104–11.

doi:10.1016/j.cattod.2017.03.048.

[37] Roy N, Sengupta R, Bhowmick AK. Modifications of carbon for polymer composites and nanocomposites. Prog Polym Sci 2012;37:781–819. doi:10.1016/j.progpolymsci.2012.02.002.

[38] Singh V, Joung D, Zhai L, Das S, Khondaker SI, Seal S. Graphene based materials: Past, present and future. Prog Mater Sci 2011;56:1178–271. doi:10.1016/j.pmatsci.2011.03.003.

[39] Han Z, Fina A. Thermal conductivity of carbon nanotubes and their polymer nanocomposites: A review. Prog Polym Sci 2011;36:914–44. doi:10.1016/j.progpolymsci.2010.11.004.

[40] Pokharel P, Lee DS. Thermal and Mechanical Properties of Reduced Graphene Oxide/Polyurethane Nanocomposite. J Nanosci Nanotechnol 2014;14:5718–21. doi:10.1166/jnn.2014.8824.

[41] Pokharel P, Pant B, Pokhrel K, Pant HR, Lim JG, Lee DS, et al. Effects of functional groups on the graphene sheet for improving the thermomechanical properties of polyurethane nanocomposites. Compos Part B Eng 2015;78:192–201. doi:10.1016/j.compositesb.2015.03.089.

[42] Salavati-Niasari M, Bazarganipour M. Effect of single-wall carbon nanotubes on direct epoxidation of cyclohexene catalyzed by new derivatives of cis-dioxomolybdenum(VI) complexes with bis-bidentate Schiff-base containing aromatic nitrogen–nitrogen linkers. J Mol Catal A Chem 2007;278:173–80. doi:10.1016/J.MOLCATA.2007.09.009.

[43] Salavati-Niasari M, Bazarganipour M. Covalent functionalization of multi-wall carbon nanotubes (MWNTs) by nickel(II) Schiff-base complex: Synthesis, characterization and liquid phase oxidation of phenol with hydrogen peroxide. Appl Surf Sci

2008;255:2963–70. doi:10.1016/J.APSUSC.2008.08.100.

[44] Bouilly D, Cabana J, Martel R. Unaltered electrical conductance in single-walled carbon nanotubes functionalized with divalent adducts. Appl Phys Lett 2012;101:053116. doi:10.1063/1.4739495.

[45] López-Bezanilla A, Triozon F, Latil S, Blase X, Roche S. Effect of the chemical functionalization on charge transport in carbon nanotubes at the mesoscopic scale. Nano Lett 2009;9:940–4. doi:10.1021/nl802798q.

[46] George J, Sreekala MS, Thomas S, Bhagawan SS, Neelakantan NR. Stress Relaxation Behavior of Short Pineapple Fiber Reinforced Polyethylene Composites. J Reinf Plast Compos 1998;17:651–72. doi:10.1177/073168449801700704.

[47] He P, Gao Y, Lian J, Wang L, Qian D, Zhao J, et al. Surface modification and ultrasonication effect on the mechanical properties of carbon nanofiber/polycarbonate composites. Compos Part A Appl Sci Manuf 2006;37:1270–5. doi:10.1016/j.compositesa.2005.08.008.

[48] Xia H, Song M. Preparation and characterization of polyurethane-carbon nanotube composites. Soft Matter 2005;1:386–94. doi:10.1039/b509038e.

[49] Araby S, Zhang L, Kuan HC, Dai J Bin, Majewski P, Ma J. A novel approach to electrically and thermally conductive elastomers using graphene. Polym (United Kingdom) 2013;54:3663–70. doi:10.1016/j.polymer.2013.05.014.

[50] Yuen SM, Ma CCM, Lin YY, Kuan HC. Preparation, morphology and properties of acid and amine modified multiwalled carbon nanotube/polyimide composite. Compos Sci Technol 2007;67:2564–73. doi:10.1016/j.compscitech.2006.12.006.

[51] Li Y, Zhu J, Wei S, Ryu J, Wang Q, Sun L, et al. Poly(propylene) Nanocomposites Containing Various Carbon Nanostructures. Macromol Chem Phys 2011;212:2429–38. doi:10.1002/macp.201100364.

[52] Y. Lan, H. Liu, X. Cao, S. Zhao, K. Dai, X. Yan, G. Zheng CL. Electrically conductive thermoplastic polyurethane/polypropylene nanocomposites with selectively distributed graphene. Polymer (Guildf) 2016;97:11–9.

[53] Wen M, Sun X, Su L, Shen J, Li J, Guo S. The electrical conductivity of carbon nanotube/carbon black/polypropylene composites prepared through multistage stretching extrusion. Polymer (Guildf) 2012;53:1602–10. doi:10.1016/j.polymer.2012.02.003.

[54] Oh JY, Jun GH, Jin S, Ryu HJ, Hong SH. Enhanced Electrical Networks of Stretchable Conductors with Small Fraction of Carbon Nanotube/Graphene Hybrid Fillers. ACS Appl Mater Interfaces 2016;8:3319–25. doi:10.1021/acsami.5b11205.

[55] Al-Saleh MH. Electrical and mechanical properties of graphene/carbon nanotube hybrid nanocomposites. Synth Met 2015;209:41–6. doi:10.1016/j.synthmet.2015.06.023.

[56] Appel AK, Thomann R, Mülhaupt R. Polyurethane nanocomposites prepared from solvent-free stable dispersions of functionalized graphene nanosheets in polyols. Polym (United Kingdom) 2012;53:4931–9. doi:10.1016/j.polymer.2012.09.016.

[57] Pokharel P, Choi S, Lee DS. The effect of hard segment length on the thermal and mechanical properties of polyurethane/graphene oxide nanocomposites. Compos Part A Appl Sci Manuf 2015;69:168–77. doi:10.1016/j.compositesa.2014.11.010.

[58] Truong Q-T, Pokharel P, Song GS, Lee D-S. Preparation and Characterization of Graphene Nanoplatelets from Natural Graphite via Intercalation and Exfoliation with Tetraalkylammoniumbromide. J Nanosci Nanotechnol 2012;12:4305–8. doi:10.1166/jnn.2012.5929.

[59] Pokharel P, Lee SH, Lee DS. Thermal, Mechanical, and Electrical Properties of Graphene Nanoplatelet/Graphene Oxide/Polyurethane Hybrid Nanocomposite. J

Nanosci Nanotechnol 2015;15:211–4. doi:10.1166/jnn.2015.8353.

[60] Pokharel P, Truong Q-T, Lee DS. Multi-step microwave reduction of graphite oxide and its use in the formation of electrically conductive graphene/epoxy composites. Compos Part B Eng 2014;64:187–93. doi:10.1016/j.compositesb.2014.04.013.

[61] Pan B, Xing B. Adsorption mechanisms of organic chemicals on carbon nanotubes. Environ Sci Technol 2008;42:9005–13. doi:10.1021/es801777n.

[62] Sulong AB, Ramli MI, Hau SL, Sahari J, Muhamad N, Suherman H. Rheological and mechanical properties of carbon nanotube/Graphite/SS316L/polypropylene nanocomposite for a conductive polymer composite. Compos Part B Eng 2013;50:54–61. doi:10.1016/j.compositesb.2013.01.022.

[63] Roland CM. Viscoelastic Behavior of Rubbery Materials. Oxford University Press; 2011. doi:10.1093/acprof:oso/9780199571574.001.0001.

[64] Pokharel P, Lee DS. High performance polyurethane nanocomposite films prepared from a masterbatch of graphene oxide in polyether polyol. Chem Eng J 2014;253:356–65. doi:10.1016/j.cej.2014.05.046.

[65] Song YS. Rheological characterization of carbon nanotubes/poly(ethylene oxide) composites. Rheol Acta 2006;46:231–8. doi:10.1007/s00397-006-0137-8.

[66] Chapartegui M, Markaide N, Florez S, Elizetxea C, Fernandez M, Santamaría A. Specific rheological and electrical features of carbon nanotube dispersions in an epoxy matrix. Compos Sci Technol 2010;70:879–84. doi:10.1016/j.compscitech.2010.02.008.

[67] Nguyen DH, Song GS, Lee DS. Effects of Colloidal Nanosilica on the Rheological Properties of Epoxy Resins Filled with Organoclay. J Nanosci Nanotechnol 2011;11:4448–51. doi:http://dx.doi.org/10.1166/jnn.2011.3685.

[68] Canales J, Muñoz ME, Fernández M, Santamaría A. Rheology, electrical conductivity and crystallinity of a polyurethane/graphene composite: Implications for its use as a

hot-melt adhesive. Compos Part A Appl Sci Manuf 2016;84:9–16. doi:10.1016/j.compositesa.2015.12.018.

[69] Liu X, Miller AL, Park S, Waletzki BE, Zhou Z, Terzic A, et al. Functionalized Carbon Nanotube and Graphene Oxide Embedded Electrically Conductive Hydrogel Synergistically Stimulates Nerve Cell Differentiation. ACS Appl Mater Interfaces 2017:acsami.7b02072. doi:10.1021/acsami.7b02072.

[70] Zhang SM, Lin L, Deng H, Gao X, Bilotti E, Peijs T, et al. Synergistic effect in conductive networks constructed with carbon nanofillers in different dimensions. Express Polym Lett 2012;6:159–68. doi:10.3144/expresspolymlett.2012.17.

[71] Ma PC, Liu MY, Zhang H, Wang SQ, Wang R, Wang K, et al. Enhanced electrical conductivity of nanocomposites containing hybrid fillers of carbon nanotubes and carbon black. ACS Appl Mater Interfaces 2009;1:1090–6. doi:10.1021/am9000503.

[72] Kudin, K.N.; Ozbas, B.; Schniepp, H.C.; Prud'Homme, R.K.; Aksay, I.A. ; Car R. Raman spectra of graphite oxide and functionalized graphene sheets. Nano Lett 2008;8:36–41.

[73] Pokharel P, Lee DS. High performance polyurethane nanocomposite films prepared from a masterbatch of graphene oxide in polyether polyol. Chem Eng J 2014;253:356–65. doi:10.1016/j.cej.2014.05.046.

[74] Pokharel P, Lee DS. Thermal and mechanical properties of reduced graphene oxide/polyurethane nanocomposite. J Nanosci Nanotechnol 2014;14:5718–21. doi:10.1166/jnn.2014.8824.

[75] Madkour TM, Hagag FM, Mamdouh W, Azzam RA. Molecular-level modeling and experimental investigation into the high performance nature and low hysteresis of thermoplastic polyurethane/multi-walled carbon nanotube nanocomposites. Polym (United Kingdom) 2012;53:5788–97. doi:10.1016/j.polymer.2012.10.041.

[76] Barick AK, Tripathy DK. Preparation, characterization and properties of acid functionalized multi-walled carbon nanotube reinforced thermoplastic polyurethane nanocomposites. Mater Sci Eng B 2011;176:1435–47. doi:10.1016/J.MSEB.2011.08.001.

[77] Young RJ, Kinloch IA, Gong L, Novoselov KS. The mechanics of graphene nanocomposites: A review. Compos Sci Technol 2012;72:1459–76. doi:10.1016/j.compscitech.2012.05.005.

[78] Pokharel P, Lee H, Lee DS. Thermal, Mechanical, and Electrical Properties of Graphene Nanoplatelet/Graphene Oxide/ Polyurethane Hybrid Nanocomposite. J Nanosci Nanotechnol 2014;15:211–4. doi:10.1166/jnn.2015.8353.

[79] Zhao J, Wu L, Zhan C, Shao Q, Guo Z, Zhang L. Overview of polymer nanocomposites: Computer simulation understanding of physical properties. Polym (United Kingdom) 2017;133:272–87. doi:10.1016/j.polymer.2017.10.035.

[80] Kim H, Miura Y, MacOsko CW. Graphene/polyurethane nanocomposites for improved gas barrier and electrical conductivity. Chem Mater 2010;22:3441–50. doi:10.1021/cm100477v.

[81] Mirzaei B, Tajvidi M, Falk RH, Felton C. Stress-relaxation behavior of lignocellulosic high-density polyethylene composites. J Reinf Plast Compos 2011;30:875–81. doi:10.1177/0731684411411337.

[82] Stan F, Fetecau C. Study of stress relaxation in polytetrafluoroethylene composites by cylindrical macroindentation. Compos Part B Eng 2013;47:298–307. doi:10.1016/j.compositesb.2012.11.008.

[83] Sreekala M., Kumaran M., Joseph R, Thomas S. Stress-relaxation behaviour in composites based on short oil-palm fibres and phenol formaldehyde resin. Compos Sci Technol 2001;61:1175–88. doi:10.1016/S0266-3538(00)00214-1.

[84] Wang Y, Cao J, Zhu L, Zhao G. Interfacial compatibility of wood flour/polypropylene composites by stress relaxation method. J Appl Polym Sci 2012;126:E89–95. doi:10.1002/app.36682.

[85] Ortiz C, K. Ober C, Kramer EJ. Stress relaxation of a main-chain, smectic, polydomain liquid crystalline elastomer. Polymer (Guildf) 1998;39:3713–8. doi:10.1016/S0032-3861(97)10321-4.

[86] Xia H, Song M, Zhang Z, Richardson M. Microphase separation, stress relaxation, and creep behavior of polyurethane nanocomposites. J Appl Polym Sci 2007;103:2992–3002. doi:10.1002/app.25462.

[87] Meera AP, Said S, Grohens Y, Luyt AS, Thomas S. Tensile Stress Relaxation Studies of TiO 2 and Nanosilica Filled Natural Rubber Composites. Ind Eng Chem Res 2009;48:3410–6. doi:10.1021/ie801494s.

[88] Siengchin S, Karger-Kocsis J. Mechanical and stress relaxation behavior of Santoprene® thermoplastic elastomer/boehmite alumina nanocomposites produced by water-mediated and direct melt compounding. Compos Part A Appl Sci Manuf 2010;41:768–73. doi:10.1016/j.compositesa.2010.02.009.

Figure Captions

Figure 1. The general fabrication route for PU nanocomposites with the hybrid of GNPs, CB and MWCNTs as nanofillers.

Figure 2. TEM micrographs of (a, b) GNPs, (c) CB and (d) MWCNTs. Scale bar 0.5 μm for (a), 10 nm for (b), 100 nm for (c,d).

Figure 3. Raman scattering spectra of (a) GNPs (b) CB and (c) MWCNTs. Disorder in the sp^2 carbon lattice of GNPs, MWCNTs and CB.

Figure 4. Steady shear viscosity of the masterbatches of carbon nanofillers (5 phr) in polyol at 60 ^oC: (a) shear viscosity versus shear rate, (b) shear viscosity versus shear stress, (c) storage modulus (G') and (d) loss modulus (G''). Strong shear thinning behavior of the carbon nanofillers in polyol in figure 4b is the indication of the network formation.

Figure 5. Electrical surface resistivity of carbon nanofillers (2.0 wt %) based PU nanocomposites. GCM112-PU2 showing lowest surface resistivity due to the formation of conductive networks by the combination of MWCNTs, GNPs and CB.

Figure 6. Stress-strain curves of single fillers based PU composites (up); (a) neat PU, (b) GNP-PU2, (c) CB-PU2, and (d) CNT-PU2. Stress-strain curves of hybrid fillers based PU composites (down); (a) neat PU, (b) GNP-CB-PU2, (c) GNP-CNT-PU2, and (d) GCM112-PU2.

Figure 7. FESEM images of (a) GNP-PU2, (b) CB-PU2,(c) CNT-PU2, (d) GNP-CNT-PU2, (e,f) GCM112-PU2. (g,h) TEM images of GCM112-PU2. Small clusters of CB were seen at the junction of CNTs and GNPs for the network formation in GCM112-PU2. Scale bar 200 nm for (a,b,c,e,f,g), 300 nm for (d) and 100 nm for (h).

Figure 8. (a) Representative diagram of stress relaxation test. (b) Stress relaxation modulus vs. time for neat PU and composites at 180 ^oC. Lower values of the stress relaxation modulus

and relaxation time of GCM112-PU2 than CNT-PU2 due to the easy broken of the network structures in hybrid composite at melt state than only CNTs entanglement in CNT-PU2.

Figure 9. Comparison of stress relaxation time at 180 ^{o}C and surface resistivity of different types of PU nanocomposites.

Figure 10. Stress relaxation modulus vs. decay time for neat PU and composites at (a) 30 ^{o}C and (b) 50 ^{o}C.

Figure 11. Plot of surface resistivity vs. stress relaxation time for neat PU and carbon nanomaterials/PU composites at 50 ^{o}C. Schematic representation of 2 wt % loading of carbon nanofillers in PU by solvent free bulk in-situ polymerization (a) GNPs, (b) MWCNTs, (c) CB and (d) GCM112.

Table Caption

Table.1

Sample code and summary on the electrical and mechanical properties of GNPs, CB, and MWCNTs based PU hybrid nanocomposites prepared by solvent free bulk *in-situ* polymerization.

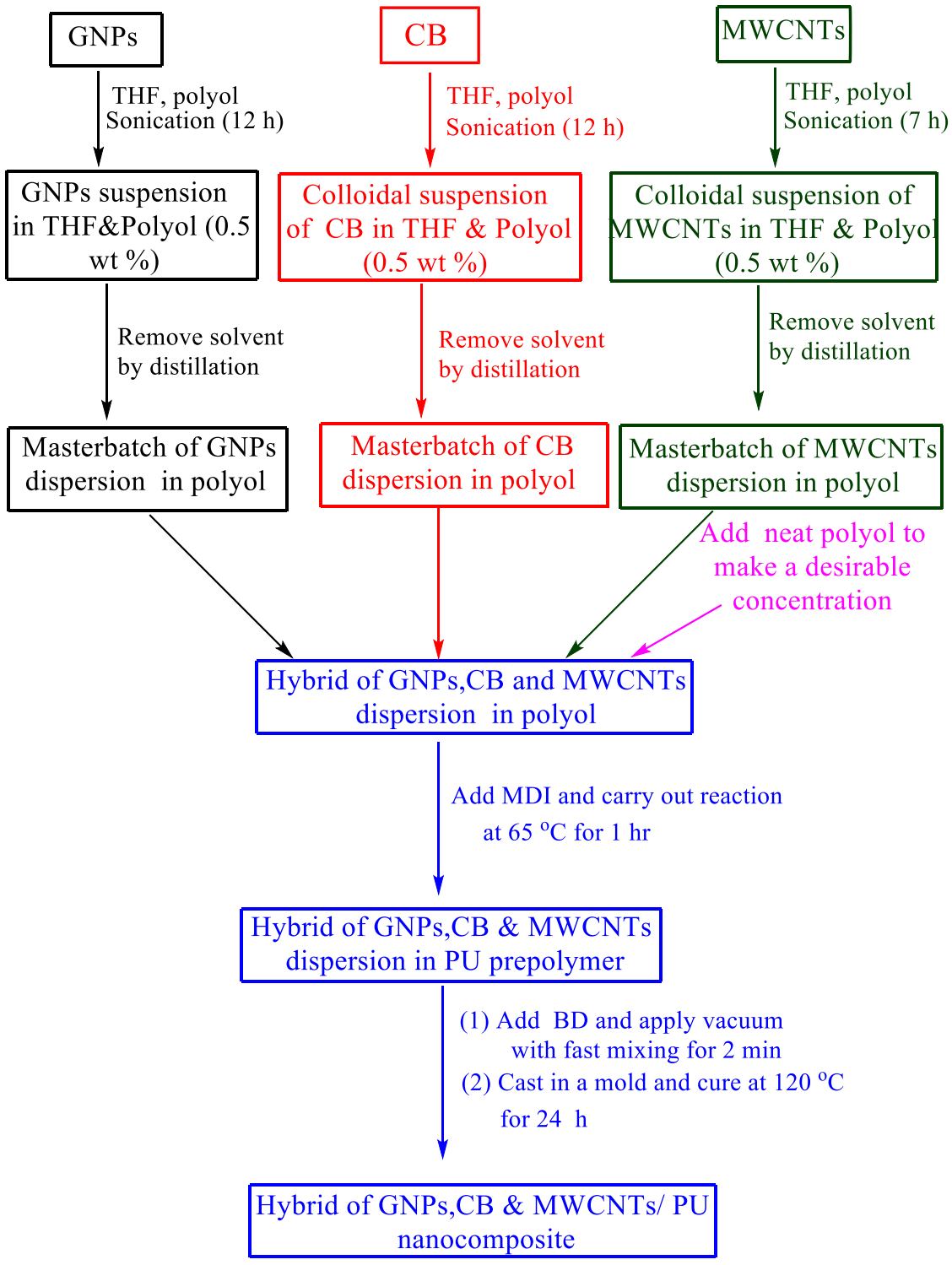
GNPs
CB
MWCNTs
THF, polyol
Sonication (12 h)
THF, polyol
Sonication (12 h)
THF, polyol
Sonication (7 h)
GNPs suspension in THF&Polyol (0.5 wt %)
Colloidal suspension of CB in THF & Polyol (0.5 wt %)
Colloidal suspension of MWCNTs in THF & Polyol (0.5 wt %)
Remove solvent by distillation
Remove solvent by distillation
Remove solvent by distillation
Masterbatch of GNPs dispersion in polyol
Masterbatch of CB dispersion in polyol
Masterbatch of MWCNTs dispersion in polyol
Add neat polyol to make a desirable concentration
Hybrid of GNPs,CB and MWCNTs dispersion in polyol
Add MDI and carry out reaction at 65 °C for 1 hr
Hybrid of GNPs,CB & MWCNTs dispersion in PU prepolymer
(1) Add BD and apply vacuum with fast mixing for 2 min
(2) Cast in a mold and cure at 120 °C for 24 h
Hybrid of GNPs,CB & MWCNTs/ PU nanocomposite

Fig. 1

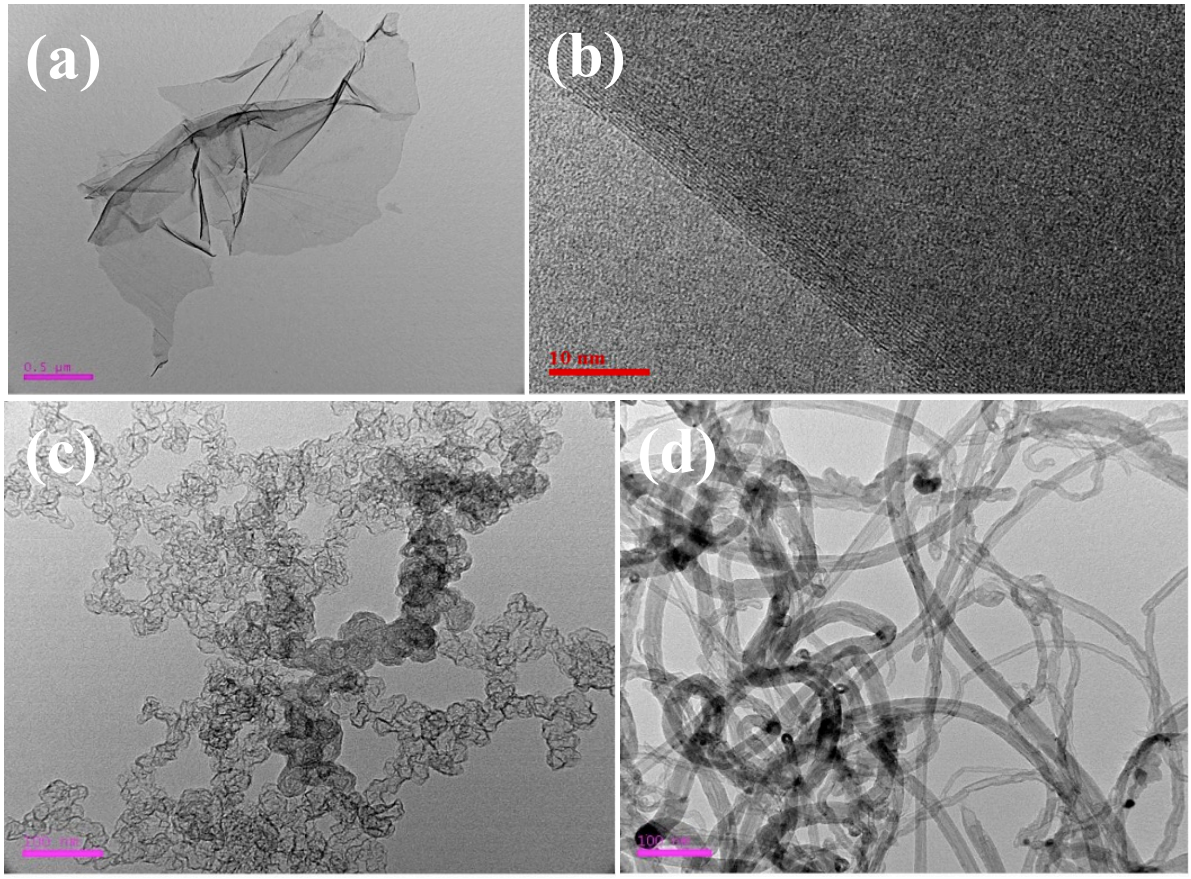

Fig. 2

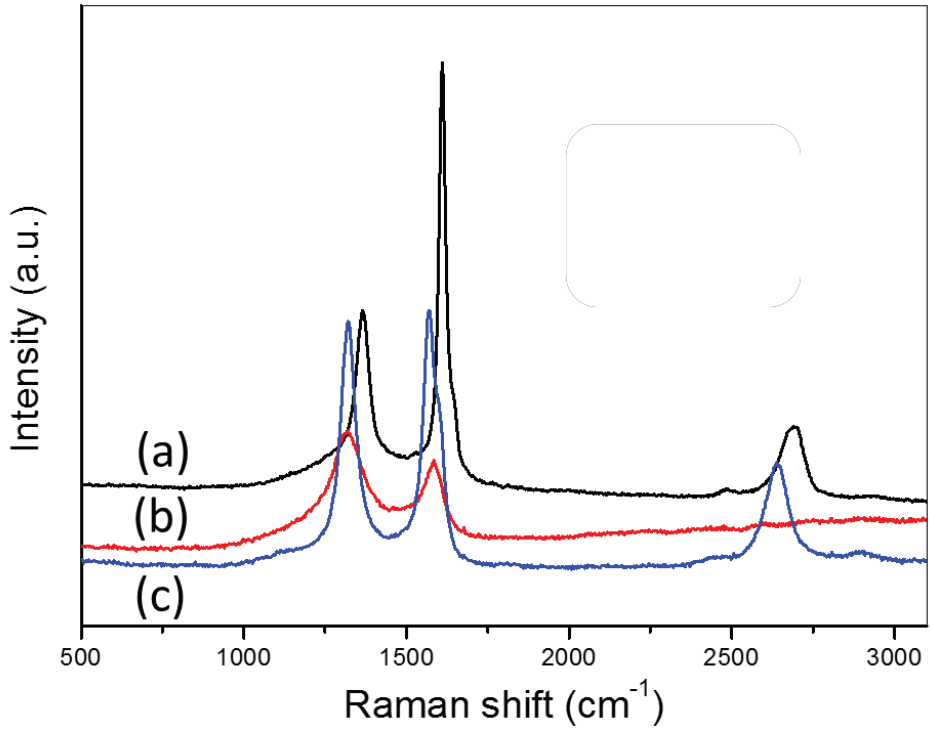
Intensity (a.u.)
(a)
(b)
(c)
500
1000
1500
2000
2500
3000
Raman shift (cm-1)

Fig. 3

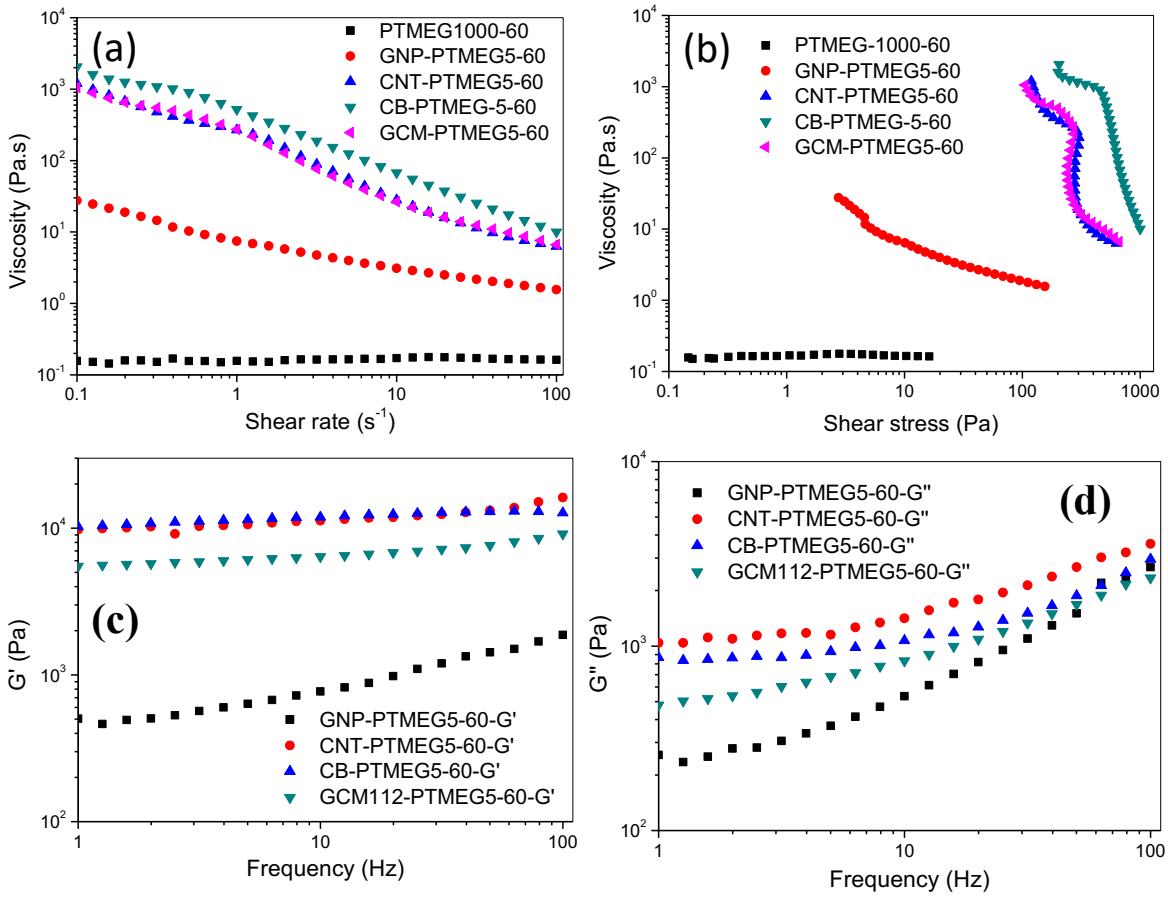
(a)
PTMEG1000-60
GNP-PTMEG5-60
CNT-PTMEG5-60
CB-PTMEG-5-60
GCM-PTMEG5-60
Viscosity (Pa.s)
Shear rate (s-1)
(b)
PTMEG-1000-60
GNP-PTMEG5-60
CNT-PTMEG5-60
CB-PTMEG-5-60
GCM-PTMEG5-60
Viscosity (Pa.s)
Shear stress (Pa)
(c)
GNP-PTMEG5-60-G'
CNT-PTMEG5-60-G'
CB-PTMEG5-60-G'
GCM112-PTMEG5-60-G'
G' (Pa)
Frequency (Hz)
(d)
GNP-PTMEG5-60-G"
CNT-PTMEG5-60-G"
CB-PTMEG5-60-G"
GCM112-PTMEG5-60-G"
G" (Pa)
Frequency (Hz)

Fig. 4

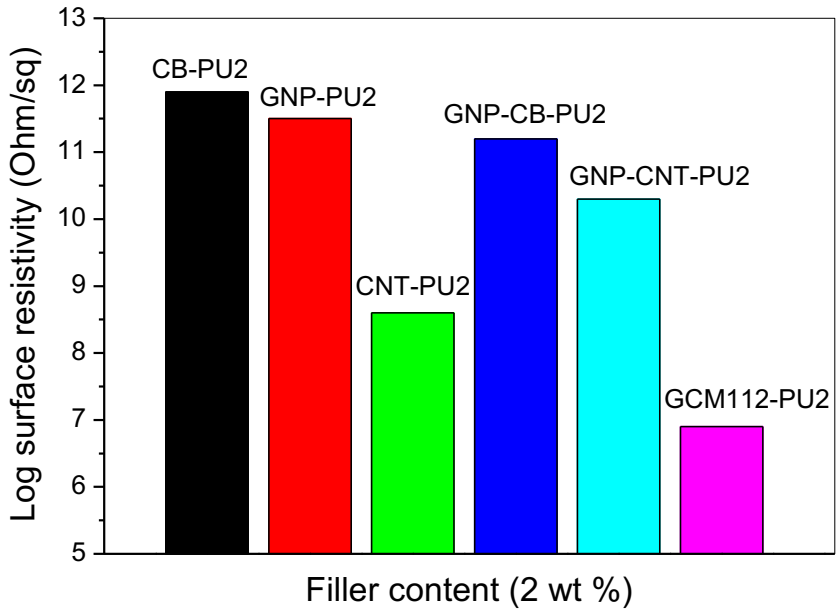
Log surface resistivity (Ohm/sq)
13
12
11
10
9
8
7
6
5
CB-PU2
GNP-PU2
CNT-PU2
GNP-CB-PU2
GNP-CNT-PU2
GCM112-PU2
Filler content (2 wt %)

Fig. 5

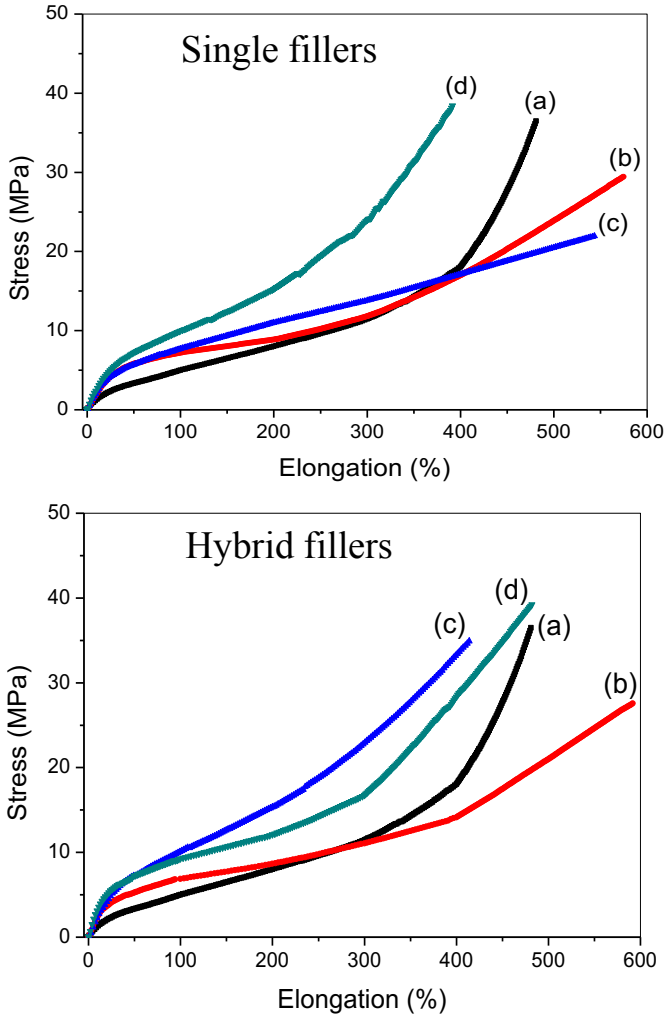
Single fillers
(d)
(a)
(b)
(c)
Stress (MPa)
Elongation (%)
0
10
20
30
40
50
0
100
200
300
400
500
600
Hybrid fillers
(c)
(d)
(a)
(b)
Stress (MPa)
Elongation (%)

Fig. 6

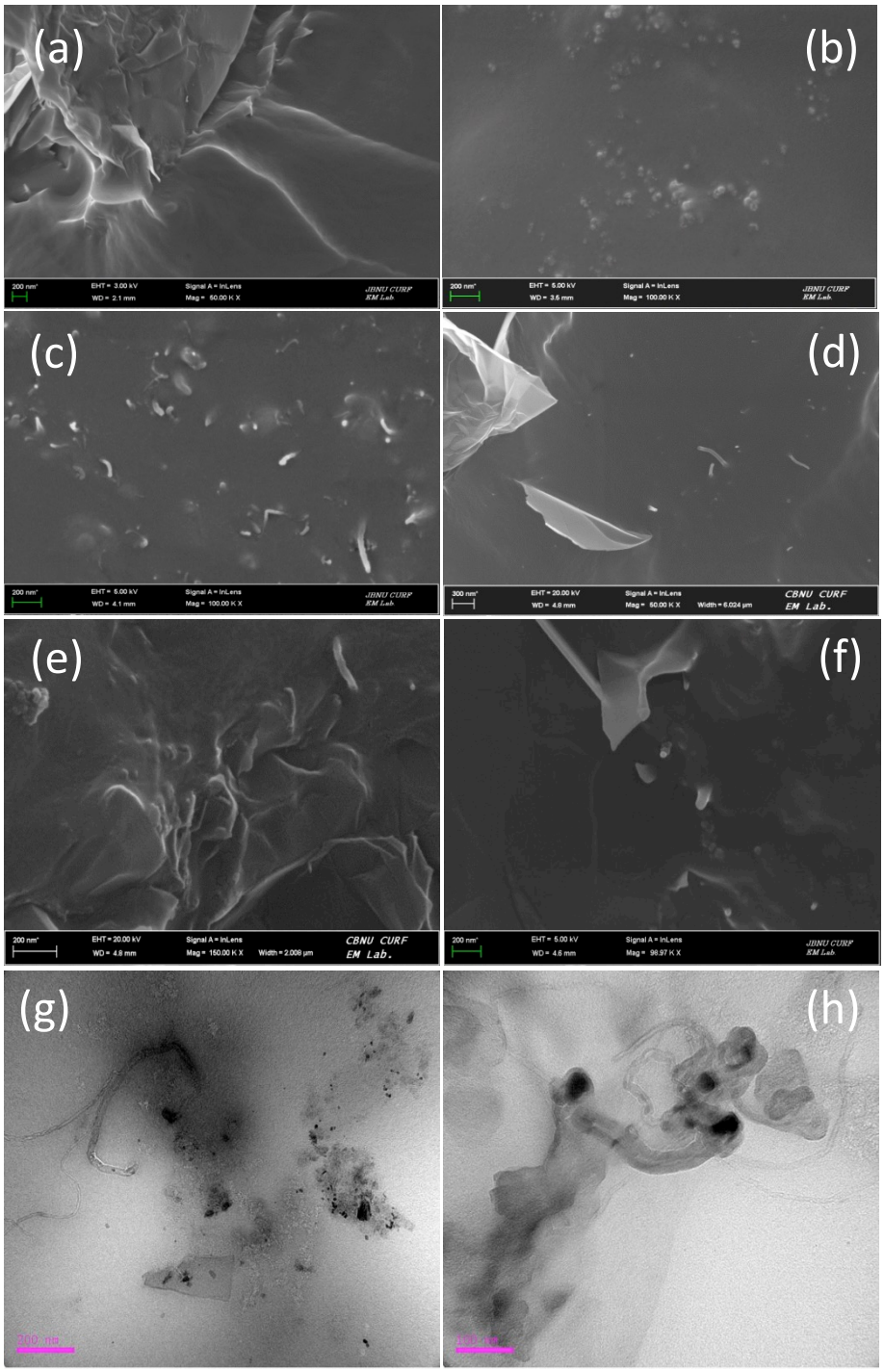

Fig. 7

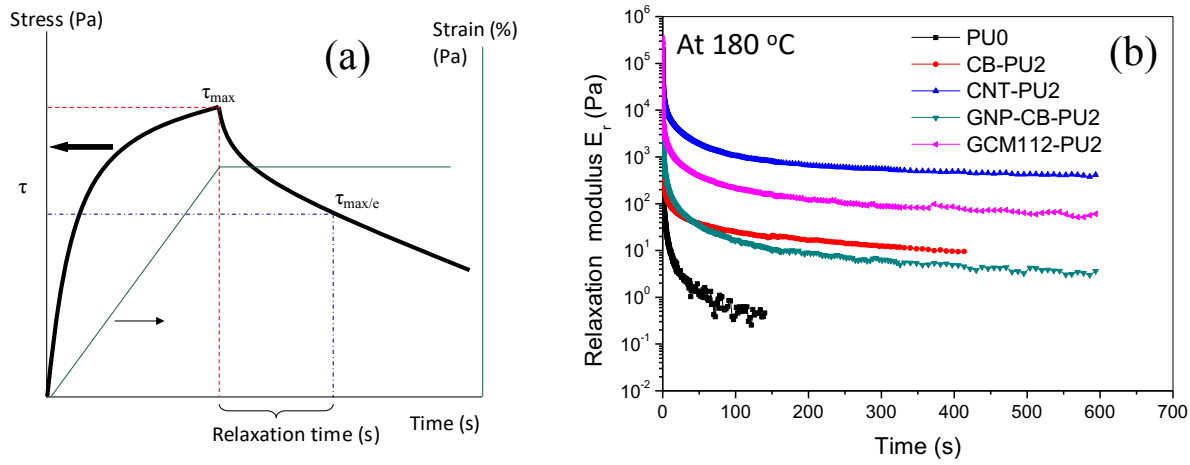
Stress (Pa)
(a)
Strain (%)
(Pa)
τmax
τ
τmax/e
Relaxation time (s)
Time (s)
At 180 °C
(b)
PU0
CB-PU2
CNT-PU2
GNP-CB-PU2
GCM112-PU2
Relaxation modulus Er (Pa)
Time (s)

Fig. 8

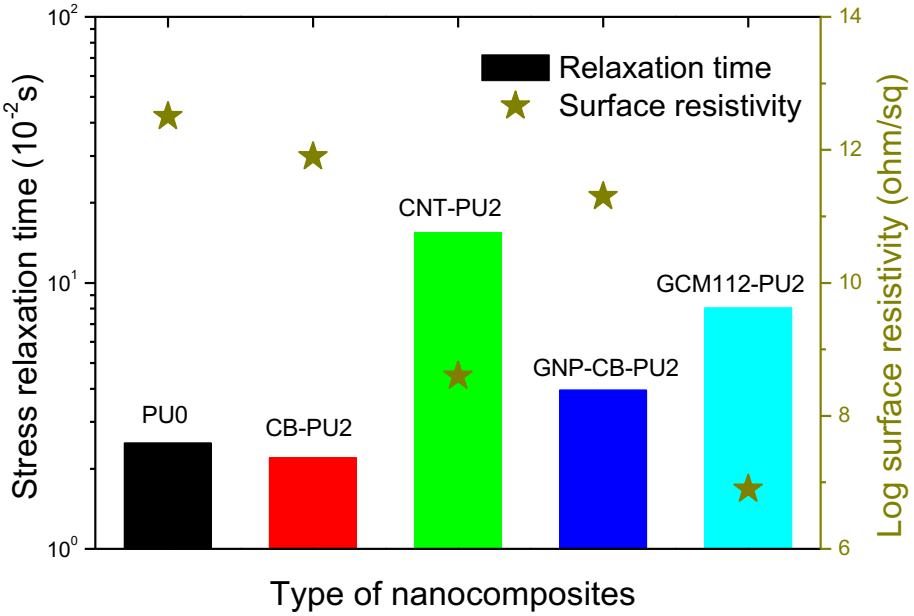
Relaxation time
Surface resistivity
CNT-PU2
GCM112-PU2
GNP-CB-PU2
PU0
CB-PU2
Stress relaxation time (10-2s)
Log surface resistivity (ohm/sq)
Type of nanocomposites
10^2
10^1
10^0
14
12
10
8
6

Fig. 9

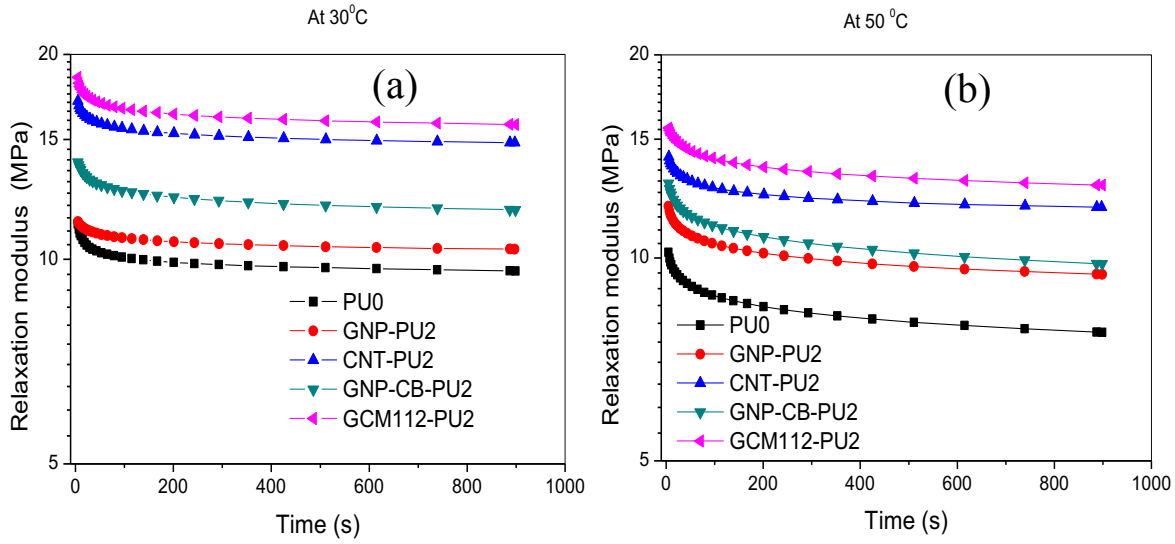
At 30°C
(a)
Relaxation modulus (MPa)
Time (s)
PU0
GNP-PU2
CNT-PU2
GNP-CB-PU2
GCM112-PU2
At 50 °C
(b)
Relaxation modulus (MPa)
Time (s)
PU0
GNP-PU2
CNT-PU2
GNP-CB-PU2
GCM112-PU2

Fig. 10

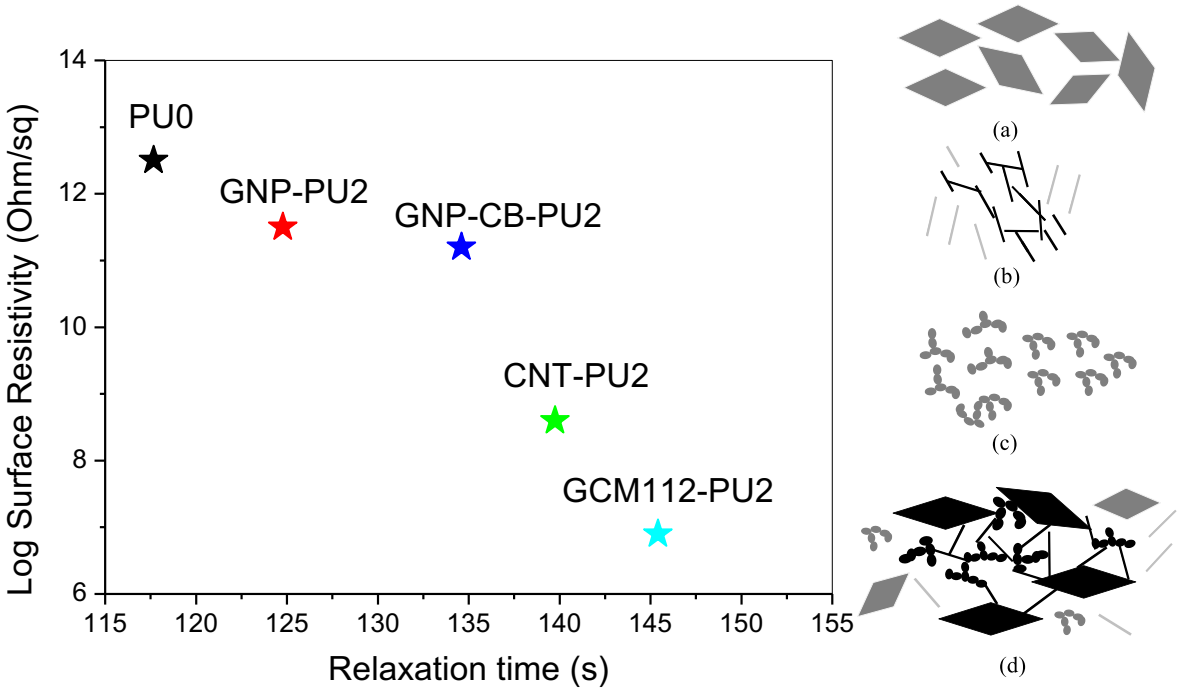
Log Surface Resistivity (Ohm/sq)
Relaxation time (s)
PU0
GNP-PU2
GNP-CB-PU2
CNT-PU2
GCM112-PU2
14
12
10
8
6
115
120
125
130
135
140
145
150
155
(a)
(b)
(c)
(d)

Fig. 11

Table. 1

Sample code	Filler (wt %)			Total filler content (wt %)	Log surf. Resistivity (Ω/□)	Tensile strength (MPa)	Young's modulus (MPa)
	GNPs	CB	CNTs				
PU0	0.0	0.0	0.0	0.0	12.5±0.3	36.48	11.92
GNP-PU1	1.0	0.0	0.0	1.0	12.5±0.4	32.56	18.25
GNP-PU2	2.0	0.0	0.0	2.0	11.5±0.4	29.43	21.44
GNP-PU3	3.0	0.0	0.0	3.0	10.1±0.5	18.83	25.16
GNP-PU5	5.0	0.0	0.0	5.0	10.0±0.4	8.5	29.34
CB-PU1	0.0	1.0	0.0	1.0	12.3±0.7	26.33	17.3
CB-PU2	0.0	2.0	0.0	2.0	11.9±0.6	21.93	22.7
CB-PU3	0.0	3.0	0.0	3.0	9.3±0.5	8.71	19.88
CNT-PU1	0.0	0.0	1.0	1.0	10.6±0.3	40.3	19.09
CNT-PU2	0.0	0.0	2.0	2.0	8.6±0.2	38.47	26.02
GNP-CB-PU2	1.0	1.0	0.0	2.0	11.2±0.5	27.54	24.2
GNP-CNT-PU2	1.0	0.0	1.0	2.0	10.3±0.3	34.7	26.8
GCM111-PU2	0.667	0.666	0.667	2.0	10.1±0.3	30.4	28.6
GCM112-PU2	0.5	0.5	1.0	2.0	6.9±0.2	39.26	35.45
GCM113-PU2	0.4	0.4	1.2	2.0	6.7±0.2	37.21	38.02
GCM211-PU2	1.0	0.5	0.5	2.0	10.7±0.5	32.4	31
GCM121-PU2	0.5	1.0	0.5	2.0	11.1±0.4	28.1	24.3